

Aalborg Universitet



AALBORG  
UNIVERSITY

## Coordinated Control of Networked AC/DC Microgrids with Adaptive Virtual Inertia and Governor-Gain for Stability Enhancement

Zhang, Yi; Sun, Qiuye; Zhou, Jianguo; Li, Linjuan; Wang, Panfeng; Guerrero, Josep M.

*Published in:*  
IEEE Transactions on Energy Conversion

*DOI (link to publication from Publisher):*  
[10.1109/TEC.2020.3011223](https://doi.org/10.1109/TEC.2020.3011223)

*Publication date:*  
2021

*Document Version*  
Accepted author manuscript, peer reviewed version

[Link to publication from Aalborg University](#)

*Citation for published version (APA):*  
Zhang, Y., Sun, Q., Zhou, J., Li, L., Wang, P., & Guerrero, J. M. (2021). Coordinated Control of Networked AC/DC Microgrids with Adaptive Virtual Inertia and Governor-Gain for Stability Enhancement. *IEEE Transactions on Energy Conversion*, 36(1), 95-110. Article 9146347. <https://doi.org/10.1109/TEC.2020.3011223>

### General rights

Copyright and moral rights for the publications made accessible in the public portal are retained by the authors and/or other copyright owners and it is a condition of accessing publications that users recognise and abide by the legal requirements associated with these rights.

- Users may download and print one copy of any publication from the public portal for the purpose of private study or research.
- You may not further distribute the material or use it for any profit-making activity or commercial gain
- You may freely distribute the URL identifying the publication in the public portal -

### Take down policy

If you believe that this document breaches copyright please contact us at [vbn@aub.aau.dk](mailto:vbn@aub.aau.dk) providing details, and we will remove access to the work immediately and investigate your claim.



# Coordinated Control of Networked AC/DC Microgrids with Adaptive Virtual Inertia and Governor-Gain for Stability Enhancement

Yi Zhang, Qiuye Sun, *Senior Member, IEEE*, Jianguo Zhou, *Member, IEEE*, Linjuan Li, Panfeng Wang and Josep M. Guerrero, *Fellow, IEEE*

**Abstract**—This paper proposes an adaptive coordinated control strategy for the networked AC/DC microgrids (MGs) to enhance the frequency and dc voltage stability of the system while keeping proper power sharing. First, a control strategy based on the synchronverter and virtual dc machine (VDCM) for the converters connecting the AC and DC MGs is proposed, which is consisted of an adaptive virtual governor and an adaptive virtual inertia regulator besides the power sharing controller. Following, in order to enhance the system stability performance, the parameter design approach of the adaptive virtual inertia and virtual governor-gain is proposed accordingly, in which the adaptive virtual inertia and virtual governor-gain are comprehensively determined by the frequency and/or dc voltage, virtual rotor speed, and rate of change of the frequency (ROCOF) and/or dc voltage (ROCOV). After that, the small-signal stability analysis of the networked AC/DC MGs with the proposed control strategy is investigated to guide the design and selection of control parameters. Finally, simulation and experimental results demonstrate that the proposed method improves the frequency/dc voltage nadir and dynamic performance of the system.

**Index Terms**—frequency and dc voltage stability, power sharing, virtual inertia, virtual governor-gain, AC/DC microgrids.

## I. INTRODUCTION

A microgrid, typically divided into three categories, i.e., AC microgrids (MGs), DC MGs and hybrid AC/DC MGs can be viewed as a small power system that facilitates the integration and application of large scale renewable energy resources (RES) [1]. Recently, hybrid AC/DC MGs gain much attention due to the combined advantages of both AC and DC MGs. The primary control objectives of the MGs including

This work was supported by National Key R&D Program of China under grant (2018YFA0702200), National Natural Science Foundation of China (61773109, 61433004, 51907098), Major Program of National Natural Foundation of China (61573094), VILLUM FONDEN under the VILLUM Investigator Grant (no. 25920): Center for Research on Microgrids (CROM). (*Corresponding authors: Qiuye Sun and Jianguo Zhou*)

Y. Zhang, Q. Sun and P. Wang are with the School of Information Science and Engineering, Northeastern University, Shenyang 110819, China (e-mail: 1810254@stu.neu.edu.cn; sunqiuye@ise.neu.edu.cn; 18540132197@163.com).

J. Zhou is with the Tsinghua-Berkeley Shenzhen Institute (TBSI), Tsinghua Shenzhen International Graduate School (TsinghuaSIGS), Tsinghua University, 518055 Shenzhen, Guangdong, P. R. China. (e-mail: jg.zhou@sz.tsinghua.edu.cn).

L. Li is with the State Grid Shandong Electric Power Co., Ltd. Linyi Power Supply Company, Linyi 276000, China (e-mail: liliniane@163.com).

J. M. Guerrero is with the Center for Research on Microgrids (CROM), Department of Energy Technology, Aalborg University, 9220 Aalborg East, Denmark (Tel: +45 2037 8262; Fax: +45 9815 1411; e-mail: joz@et.aau.dk)

hybrid AC/DC MGs mainly contain power sharing [2], [3], voltage/frequency regulation and stability maintaining [4].

Among these objectives, power sharing among distributed generators (DGs) or MGs is one of the key issues. Droop control [4] has been widely accepted and applied in DGs within a MG. Further, this topic in hybrid AC/DC MGs has been extensively discussed [5]–[8]. For example, in [7], a bidirectional droop control scheme was proposed to control the interlinking converters (ICs) to achieve proportional power sharing between AC and DC subgrids. The above works mainly discuss power sharing of a hybrid AC/DC MG consisting of one AC and one DC subgrid. Power sharing among multiple MGs within a cluster is also important and necessary for operation reliability and flexibility. Recently, some results on this topic have been reported in [3], [9]–[11]. However, these works only consider DC MG [9] or AC MG [11] clusters without ICs' connection or hybrid MGs [3], [10] connected by bidirectional DC-AC ICs in parallel. In the future, a large number of different types of MGs can be developed in the distributions system. They can be interconnected by DC-AC and DC-DC ICs which can be formed as a complicated multi-terminal direct current (MTDC) system. Therefore, we mainly concentrate on power sharing among the networked AC/DC MGs connected by MTDC system where DC-AC and DC-DC ICs are used, which has not been well discussed.

Stability issue is another equally important problem for the MG. High penetration of power converters drastically reduces the inertia of MGs, seriously threatening system stability. Inertia [12] and turbine-governor response speed [13] are two key factors to determine the system stability. Currently, inertia emulation, e.g., virtual synchronous generator (VSG) technology [14], is a promising solution to address this issue. Existing research can be divided into two categories: *fixed inertia* and *adaptive inertia*. Regarding the *first* category, methods currently mainly concentrate on VSG itself and applications within MGs [14]–[16]. For instance, a virtual inertia control strategy for DC MGs through bidirectional grid-connected converters was proposed to provide inertia for the dc bus voltage [15], but this approach cannot provide inertia when the MGs are off-grid. For hybrid AC/DC system, several research works have been reported in literature [17]–[19]. Qi et al. [17] and E. Rakhshani et al. [18] proposed control strategies based on VSGs and derivative control technique, respectively, to enhance the stability performance during loading changes. In [19], a ratio-based selective inertial and primary frequency

support was developed through MTDC grids with offshore wind farms. These works, however, mainly focus on fixed inertia that cannot be adjusted adaptively according to the system disturbance. This may not result in good performance. It can be reasonable that a relatively large inertia should be provided for the system under a large disturbance to guarantee system stability while a relatively small inertia is required under a small disturbance for fast response speed.

Therefore, the *second* category, adaptive virtual inertia control, is reported in literature [20]–[30]. A representative research work is [21] where two independent values of virtual inertia were selected based on judging the states of the relative angular velocity difference and its change rate. However, only two values of inertia can be selected and the influence of frequency derivative term is also neglected. In [20], a self-tuning algorithm was proposed to support dynamic frequency control by continuously searching for the optimal inertia constant and damping constant during frequency transients. But the nonlinear nature of adaptive inertia control is easy to affect the stability of power systems. Following, similar/improved adaptive inertia control schemes were developed, such as that based on bang-bang control [23], dual-adaptive inertia control to improve the overall performance of power and frequency [24] and that in [25] where the nominal constant inertia need to be set large enough to avoid negative inertia. In [26], an inertial response strategy was proposed for the IC based on adaptive droop control approach. The IC can provide inertial power for the DC grid by adaptively swinging the droop curve according to the variation of the dc bus voltage. The inertial response performance in this approach, however, comes from droop regulation in essence but not the inertia itself, which is more similar to governor-gain regulation. Some similar works can be found in the published literature [27] and [28] for the wind turbine generator (WTG) system and WTG/energy storage (ES) system, respectively, to provide short-term frequency support. From the point of view of optimal control, U. Markovic *et al.* [29] designed optimal state feedback gain to adaptively adjust the virtual inertia and damping constants using linear quadratic regulator (LQR)-based optimization technique. Recently, some intelligent control algorithms were also developed. For instance, A. S. Mir *et al.* [30] developed a self-tuning neural predictive control scheme to adaptively obtain optimal emulated inertia and damping for an ultrabattery energy storage system. However, we can find that the works reviewed above also primarily concentrate on VSG itself and applications in MGs. Applications of adaptive virtual inertia in ICs in networked AC/DC MGs have not been reported. Therefore, we do this research to make up this gap.

Motivated by the above inspirations, this paper focuses on presenting the architecture and control scheme of the networked AC/DC MGs in order to realize the optimal utilization of RES and enhance the stability of the system while keeping proper power sharing. In comparison with the previous research articles, the main contributions of this paper are summarized as follows:

1) The MTDC-based networked AC/DC MGs architecture increases the flexible interaction among multiple AC and DC MGs so that the ability to reliability of system and utilization

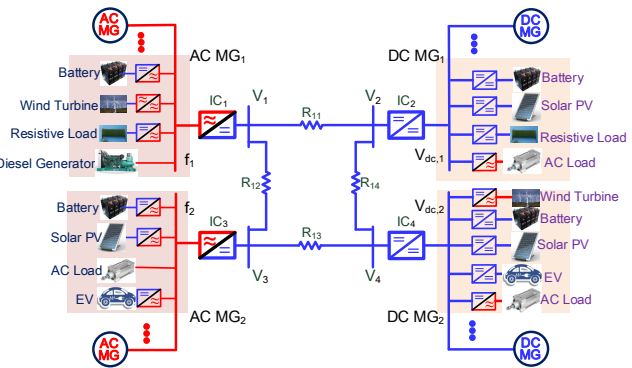


Fig. 1. A possible layout of the networked AC/DC MGs connected by low voltage MTDC.

of RES is greatly enhanced.

2) The adaptive coordinated control scheme for the networked AC/DC MGs connected by MTDC is proposed to simultaneously achieve proper power sharing among MGs and enhance the frequency and dc voltage stability, which is different from [20]–[30] where the adaptive schemes are mainly designed for DGs within MGs and [17]–[19] where the virtual inertia and damping are fixed for ICs in the hybrid AC/DC systems.

3) Unlike [23] and [25], the proposed adaptive scheme has continuous regulation ability and can quickly provide large inertia and gain when disturbance occurs. Both the time-domain simulation and the frequency-domain modal analysis are applied to show the influences of the virtual inertia and virtual governor-gain on system stability.

The remainder of this paper is organized as follows. The structure of the networked AC/DC MG is briefly introduced in section II. Section III presents the proposed power sharing among the networked MGs. Detailed IC controller design with adaptive virtual inertia and virtual governor-gain is given in section IV, and the corresponding parameter design of the virtual inertia and virtual governor-gain is presented. Section V investigates the small-signal analysis of the networked AC/DC MGs with the proposed control strategy. Simulation and experimental results are presented in Section VI and Section VII. Conclusions are drawn in Section VIII.

## II. SYSTEM STRUCTURE

A possible layout of the networked AC/DC MGs connected by low voltage MTDC is shown in Fig. 1, in which two AC MG clusters and two DC MG clusters are considered. Each AC or DC MG cluster can be composed of several MGs located in a close vicinity. Each MG has its own sources, storages and loads. For instance, in remote suburbs or countryside, there are many villages. If each of these villages is developed into a MG, then several of them equipped with the same type of MG in a close vicinity can be interconnected to form a MG cluster. And these MG clusters can also be tied together via power converters for enhancing system reliability and utilization of RES. The formed networked AC/DC MGs can run in grid-connected and interconnected (the formed networked MGs are disconnected from the utility grid) modes, each MG can

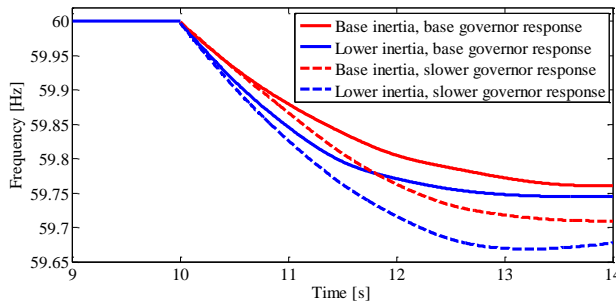


Fig. 2. The nadir of arrested frequency is mainly determined by the system inertia and the governor response speed besides the amount of load change [13].

also run in islanded mode. In this paper, we only consider the interconnected mode.

Note that there may be an imbalance between the power generation and load of each MG, that is, some MGs may generate a lot of power, but their load is very small, and some MGs have the opposite situation. On the other hand, the networked AC/DC MGs are full of RES with a large number of power electronic interfaces, which results in low inertia and poor system stability. Therefore, in order to ensure reliable operation and stability of the system, a power management approach that can provide adaptive virtual inertia and virtual governor-gain support to enhance the stability of the networked AC/DC MGs while keeping power sharing among these MGs will be proposed in this paper. More details will be discussed in the following sections.

### III. POWER SHARING AMONG THE NETWORKED MGs

For an AC MG with at least two paralleled DGs [5], droop control scheme has been widely used. The total active power and reactive power demand, in principle, can be shared by DGs in the AC MG according to their respective rated power ratios. Based on the linearity of the droop equation, the aggregated equivalent droop control equation for each AC MG can be written as [2]

$$\begin{cases} f_{ac,m} = f_{ac,m}^* - m_{ac,m} P_{ac,m} \\ V_{ac,m} = V_{ac,m}^* - n_{ac,m} Q_{ac,m} \end{cases} \quad (1)$$

where  $P_{ac,m}$  and  $Q_{ac,m}$  are the total actual output active power and the reactive power of all the DGs within the  $m$ th AC MG, respectively;  $f_{ac,m}^*$  and  $V_{ac,m}^*$  are the rated operating angular frequency and the voltage amplitude, respectively;  $f_{ac,m}$  and  $V_{ac,m}$  represent the output reference angular frequency and the voltage reference amplitude, respectively;  $m_{ac,m}$  and  $n_{ac,m}$  are the combined droop coefficients.

Similar to the AC MG, the aggregated equivalent droop control equation for each DC MG can be written as [7]

$$V_{dc,n} = V_{dc,n}^* - k_{dc,n} P_{dc,n} \quad (2)$$

where  $P_{dc,n}$  is the total actual output active power of all the DGs within the  $n$ th DC MG;  $V_{dc,n}^*$  and  $V_{dc,n}$  are the rated operating voltage and the output voltage reference amplitude, respectively;  $k_{dc,n}$  is the droop coefficient.

Applying the principle of droop control of DGs to the networked MGs to achieve power sharing among these MGs

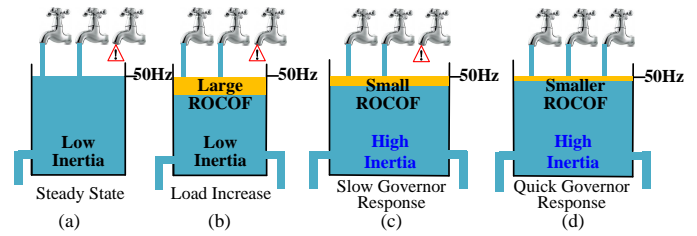


Fig. 3. The effect of the system inertia and the governor response speed on ROCOF.

means maintaining the per-unit value of the AC MG frequency equal to the per-unit value of the DC MG voltage [5], [7], i.e.,

$$f_{m,pu} = V_{dc,n,pu} \quad (3)$$

where  $f_{m,pu}$  and  $V_{dc,n,pu}$  represent the per-unit values of the frequency and the dc voltage of the  $m$ th AC MG and the  $n$ th DC MG, respectively. The per-unit values  $x_{pu}$  can be calculated by using  $x_{pu} = \frac{x - 0.5(x_{max} + x_{min})}{0.5(x_{max} - x_{min})}$ , where  $x$  is the ac frequency and the dc voltage,  $x_{max}$  and  $x_{min}$  are the maximum and minimum values. More details can be found in [5], [7]. Therefore, the control equation of power sharing for the networked AC/DC MGs proposed in this paper can be given as

$$P_{trans,i} = \left( k_{P,i} + \frac{k_{I,i}}{s} \right) (\varsigma_i - V_{com,pu}) \quad (4)$$

where  $\varsigma_i$  represents  $f_{m,pu}$  or  $V_{dc,n,pu}$ ;  $P_{trans,i}$  is the transferred active power by the DC-AC or DC-DC IC;  $k_{P,i}$  and  $k_{I,i}$  are proportional and integral coefficient,  $V_{com,pu} = V_{1,pu}$ . Then, when the system reaches the steady state, there is  $\varsigma_i \rightarrow V_{com,pu}$ , that is  $f_{1,pu} = f_{2,pu} = V_{dc,1,pu} = V_{dc,2,pu}$ , the power sharing in the the networked AC/DC MGs is realized.

### IV. ADAPTIVE CONTROL STRATEGY OF THE NETWORKED AC/DC MGs

As mentioned above, a large number of low-inertia power electronic converters used can deteriorate of the networked AC/DC MGs. In this section, therefore, we further enhance the system stability with the proposed adaptive virtual inertia and virtual governor-gain approach based on the models of the synchronverter [14] and VDCM [15].

In principle, the stability of the system can be reflected by the arresting time of the primary frequency and dc voltage mainly determined by the effective inertia constant of the system and the increase rate of generation besides the amount of load change. As can be seen from Fig. 2, the larger inertia and faster governor response, the better frequency performance can be achieved [13].

Therefore, this paper proposes a method to simultaneously adaptively adjust the virtual inertia and the virtual governor-gain to improve the system stability. Further, using Fig. 3, we will illustrate this idea that how the relationship between the system inertia and the increase rate of generation affect the frequency and dc voltage of the networked AC/DC MGs through the analogy of water following into and out of a container. If the power generation and load in the networked AC/DC MGs are exactly balanced (water inflow and outflow

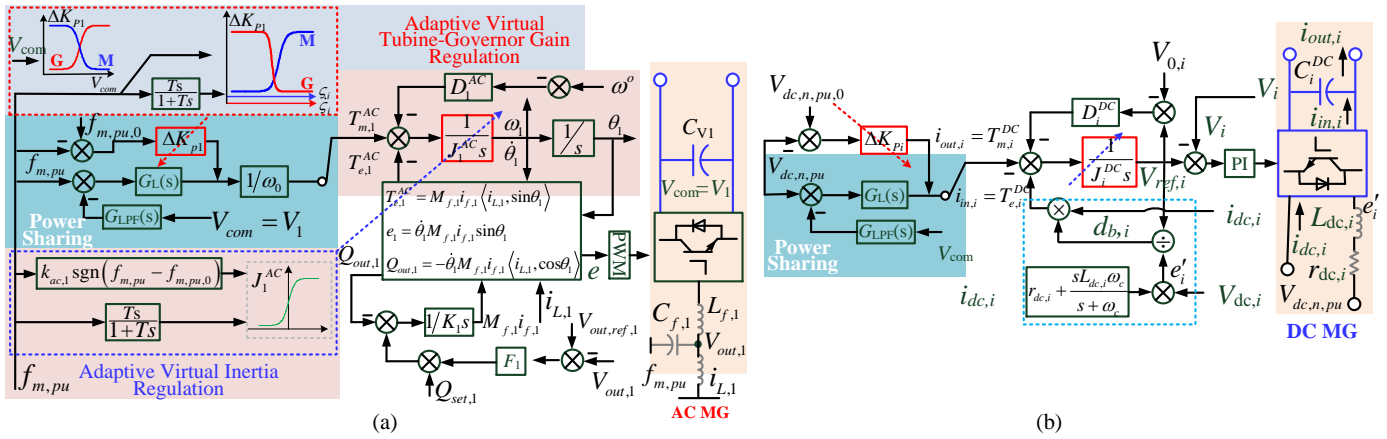


Fig. 4. Proposed frequency and dc voltage support scheme associated with the adaptive virtual and virtual governor-gain. (a) Control block diagram of the DC-AC IC. (b) Control block diagram of the DC-DC IC.

are equal), the frequency (dc voltage) will stabilize at 50 Hz (120 V) as shown in Fig. 3(a). If the load in the AC MG increases dramatically (outflow begins to exceed inflow), frequency will fall fast below 50 Hz (large rate of change of frequency (large ROCOF)) due to its low system inertia, as seen in Fig. 3(b). To address this issue, we take measures from two aspects. On the one hand, the system inertia is adaptively increased by controlling the DC- AC IC connected to the AC MG in the MTDC, which will allow the frequency to fall slowly (small ROCOF) shown in Fig. 3(c). On the other hand, besides increasing the system inertia, we further appropriately increase the rate of generation by adaptively adjusting water tank valves (virtual governor-gain), i.e., injecting more water from the other box (MG) into the water box more quickly (see Fig. 3(d)). With this measure, the frequency will fall more slowly (smaller ROCOF) than the system that only increases inertia, which means that better frequency stability performance can be achieved (see Fig. 3(d)).

#### A. IC Controllers with Adaptive Virtual Inertia and Virtual Governor-Gain

The overall control block diagram of the IC is shown in Fig. 4, where Fig. 4(a) shows the DC-AC IC control strategy while Fig. 4(b) shows the DC-DC IC control strategy. The control strategy is based on the synchronverter and VDCM. Besides the power sharing controller, the proposed control method also includes two parts: 1) adaptive virtual inertia regulation scheme and 2) adaptive virtual governor-gain regulation scheme, which are shown in Fig. 4(a) but not shown in Fig. 4(b) for DC-DC IC due to the similar control structure.

1) DC-AC IC controller: From Fig. 4(a), the DC-AC IC controller can be mathematically written as

$$\begin{aligned} J_i^{AC} \frac{d\omega_i}{dt} &= T_{m,i}^{AC} - T_{e,i}^{AC} - D_i^{AC} (\omega_i - \omega_0) \\ K_i \frac{dM_{f,i} i_{f,i}}{dt} &= F_i (V_{out,ref,i} - V_{out,i}) + Q_{set,i} - Q_{out,i} \end{aligned} \quad (5)$$

where  $J_i^{AC}$  and  $D_i^{AC}$  are the adaptive virtual inertia and the frequency damping coefficient, respectively;  $\omega_i$  is the

rotating speed of the virtual rotor and  $\omega_0$  is its reference value.  $T_{m,i}^{AC}$  and  $T_{e,i}^{AC}$  are the virtual mechanical and electromagnetic torque, respectively.  $M_{f,i}$  and  $i_{f,i}$  are the maximum mutual inductance and the field excitation current, respectively;  $K_i$  and  $F_i$  are the integral gain and the voltage droop coefficient, respectively;  $V_{out,ref,i}$  and  $V_{out,i}$  are reference voltage and output voltage, respectively;  $Q_{set,i}$  and  $Q_{out,i}$  are the reactive power set point and output, respectively.  $T_{e,i}^{AC}$  and internal voltage  $e_i$  are given by  $T_{e,i}^{AC} = M_{f,i} i_{f,i} \langle i_{L,i}, \tilde{\sin\theta}_i \rangle$ ,  $e_i = \dot{\theta}_i M_{f,i} i_{f,i} \tilde{\sin\theta}_i$  [14].

The virtual mechanical torque  $T_{m,i}^{AC}$  is given by

$$T_{m,i}^{AC} = \frac{P_{trans,i} + \overbrace{\Delta K_{pi} (f_{m,pu,0} - f_{m,pu})}^{\text{Virtual Governor}}}{\omega_0} \quad (6)$$

where  $P_{trans,i}$  is the active power transferred by IC for power sharing among MGs, which can be obtained from equation (4);  $\Delta K_{pi} (f_{m,pu,0} - f_{m,pu})$  is the virtual governor part and  $\Delta K_{pi}$  is the adaptive virtual governor-gain.

2) DC-DC IC controller: Similar to the DC-AC IC controller, the DC-DC IC controller based on the VDCM is as

$$\begin{aligned} J_i^{DC} \frac{dV_{ref,i}}{dt} &= T_{e,i}^{DC} - D_i^{DC} (V_{ref,i} - V_{0,i}) \\ &\quad - \frac{P_{trans,i} + \overbrace{\Delta K_{pi} (V_{dc,n,pu,0} - V_{dc,n,pu})}^{\text{Virtual Governor}}}{V_{0,i}} \end{aligned} \quad (7)$$

where  $J_i^{DC}$  and  $D_i^{DC}$  are the adaptive virtual inertia and the voltage droop coefficient, respectively;  $P_{trans,i}$  is the active power transferred by IC for power sharing among MGs, which is also obtained from equation (4);  $V_{ref,i}$  is the output reference value of the VDCM and  $V_{0,i}$  is its set point;  $T_{e,i}^{DC}$  is the virtual electrical torque given by [31]

$$T_{e,i}^{DC} = i_{dc,i} V_{ref,i} \left( V_{dc,i} - i_{dc,i} \left( r_{dc,i} + \frac{sL_{dc,i}\omega_c}{s + \omega_c} \right) \right)^{-1} \quad (8)$$

where  $i_{in,i}$  and  $i_{dc,i}$  are the VDCM input current and the filter inductor current, respectively;  $d_{b,i}$  is the duty cycle of the switch in the VDCM;  $r_{dc,i}$ ,  $L_{dc,i}$  and  $\omega_c$  are the resistance,

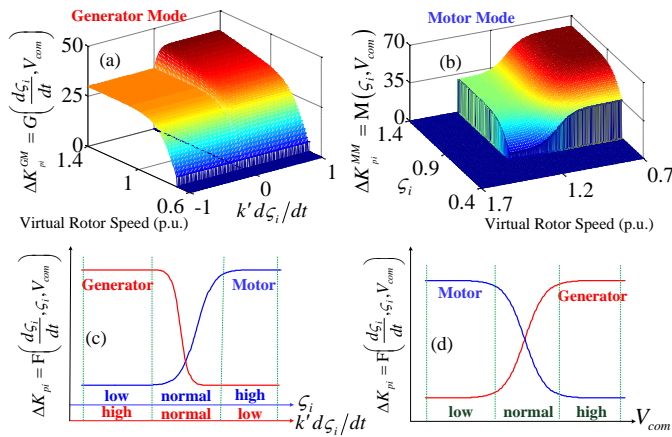


Fig. 5. Determination of adaptive virtual governor-gain in the proposed strategy. (a) Relationship among  $\Delta K_{pi}^{GM}$ ,  $V_{com}$  and  $k' \frac{d\zeta_i}{dt}$ . (b) Relationship among  $\Delta K_{pi}^{MM}$ ,  $V_{com}$  and  $\zeta_i$ . (c) Curve of  $\Delta K_{pi}$  when  $V_{com} = 1$ . (d) Curve of  $\Delta K_{pi}$  when  $k' \frac{d\zeta_i}{dt} = 0.5$  and  $\zeta_i = 0.8$ .

inductance and cut-off frequency of the filter, respectively;  $V_{dc,i}$  is the dc bus voltage of the DC MG.

With this control method, the frequency and dc voltage stability will be improved while keeping power sharing for the AC/DC MGs. In the following, we will focus on the parameter design of the virtual inertia and virtual governor-gain.

## B. Design of Adaptive Virtual Inertia and Virtual Governor-Gain

### 1) Design of Adaptive Virtual Inertia

As we know, the rate of change of the frequency (ROCOF) and/or dc voltage (ROCOV) reflects both the disturbance scale caused by the amount of load and/or source change and the system inertia level. The larger disturbance will result in higher ROCOF and/or ROCOV, which means the frequency and/or dc voltage drop rapidly at the beginning stage. Therefore, during the “arresting period”, the choice of inertia should be that the greater disturbance to the system, the greater inertia should be provided to suppress the rapid decline of ROCOF and/or ROCOV. Conversely, the smaller disturbance to the system, the less inertia should be provided. On the other hand, during the “rebound period”, the frequency and/or dc voltage is expected to be quickly restored to the steady state value. Therefore, the inertia at this time should be small enough.

In view of the above analysis, the  $J_i$  can be given as

$$J_i = \begin{cases} J_{i0} + (J_{i,\max} - J_{i0}) \tanh(k' \frac{d\zeta_i}{dt}) & k' \frac{d\zeta_i}{dt} \geq 0 \\ J_{i0} + (J_{i0} - J_{i,\min}) \tanh(k' \frac{d\zeta_i}{dt}) & k' \frac{d\zeta_i}{dt} < 0 \end{cases} \quad (9)$$

where  $k' = k_i \text{sgn}(\zeta_i - \zeta_{i0})$ ,  $k_i$  represents  $k_{ac,i}$  (DC-AC IC) or  $k_{dc,i}$  (DC-DC IC);  $k_{ac,i}$  and  $k_{dc,i}$  are adjustable constants;  $J_{i0}$  is the value of  $J_i$  at the steady state;  $J_{i,\max}$  and  $J_{i,\min}$  represent the minimum and maximum values of  $J_i$ , respectively.

From (9), we can find that the ROCOF and/or ROCOV are maximum when the system is disturbed, i.e.,  $k' \frac{d\zeta_i}{dt}$  is located at the far right of the horizontal axis where a large inertia coefficient corresponds to it, proving that it meets our analysis

above. As the ROCOF and/or ROCOV decrease, the inertia coefficient also slowly decreases to  $J_{i0}$  until the ROCOF and/or ROCOV are equal to zero. When  $k' \frac{d\zeta_i}{dt}$  is less than 0, the inertia coefficient continues to decrease, which ensures that the system has a good dynamic response during the “rebound period”.

### 2) Design of Adaptive Virtual Governor-Gain

As mentioned earlier, in addition to the inertia, the response speed of the virtual governor also affects the stability of the system frequency and/or dc voltage under disturbances. Therefore, in this subsection, we need to design a method to adaptively adjust the response speed of the virtual governor for these converters in the MTDC to further improve the system stability.

Each converter can operate in two different modes under disturbances, one is the generator mode (GM) and the other is the motor mode (MM). For example, when the load in one of the networked AC/DC MGs suddenly changes, if the converter connected to it injects power into the disturbed MG, it operates in the GM and vice versa. Thus, for the GM, the design of virtual governor-gain should be based on the ROCOF and/or ROCOV and the virtual rotor speed. Large ROCOF and/or ROCOV require fast response speed of the virtual governor while high virtual rotor speed can provide large kinetic energy for the virtual generator to absorb, resulting in fast support of primary frequency and dc voltage. For the MM, the design of virtual governor-gain should be based on the virtual rotor speed and the frequency and/or dc voltage. Large virtual rotor speed reflects large virtual kinetic energy, therefore the converter operating in the MM does not need to provide more power. On the other hand, large frequency and/or dc voltage reflect that much more power can be provided by undisturbed MGs. Therefore, the virtual governor-gain in the GM should be designed to be larger when the virtual rotor speed and the ROCOF and/or ROCOV are relatively large and vice versa, and in the MM, the virtual governor-gain should be designed to be larger when the virtual rotor speed is relatively small and frequency and/or dc voltage are relatively large and vice versa. Therefore, according to the above ideas, the virtual governor-gain  $\Delta K_{pi}$ , divided into  $\Delta K_{pi}^{GM}$  and  $\Delta K_{pi}^{MM}$ , is designed as follows.

$$\Delta K_{pi} = F\left(\frac{d\zeta_i}{dt}, \zeta_i, V_{com}\right) = \begin{cases} G\left(\frac{d\zeta_i}{dt}, V_{com}\right), & \text{GM} \\ M\left(\zeta_i, V_{com}\right), & \text{MM} \end{cases} \quad (10)$$

For the GM, the virtual governor-gain  $\Delta K_{pi}^{GM}$  can be given as

$$\Delta K_{pi}^{GM} = G\left(\frac{d\zeta_i}{dt}, V_{com}\right) = \begin{cases} \left( \frac{\eta_i (\tanh(m_i k' \frac{d\zeta_i}{dt})) V +}{r_i \tanh(d_i V) + \Delta K_{pi,0}^{GM}} \right) V, & k' \frac{d\zeta_i}{dt} > 0 \\ r_i \tanh(d_i V) + \Delta K_{pi,0}^{GM}, & k' \frac{d\zeta_i}{dt} < 0 \\ 0, & V_{com} < V_{com,\min} \end{cases} \quad (11)$$

where  $G\left(\frac{d\zeta_i}{dt}, V_{com}\right)$  is the gain function, which describes the influence of  $\frac{d\zeta_i}{dt}$  and  $V_{com}$  on  $\Delta K_{pi}^{GM}$ ;  $V = V_{com} - V_{com,\min}$ ,  $V_{com,\min}$  and  $V_{com,\max}$  represent the minimum and maximum values of  $V_{com}$ , respectively;  $\Delta K_{pi,0}^{GM}$  is the value of  $\Delta K_{pi}^{GM}$  at

the steady state;  $\eta_i$ ,  $m_i$ ,  $r_i$  and  $d_i$  are all adjustable constants.

On the other hand, for the MM, the virtual governor-gain  $\Delta K_{pi}^{MM}$  can be given as

$$\Delta K_{pi}^{MM} = M(\varsigma_i, V_{com}) = \begin{cases} \begin{pmatrix} -\beta_i \tanh(l_i V') \\ +\alpha_i \tanh(q_i \varsigma') \\ +\Delta K_{pi,0}^{MM} \end{pmatrix}, \varsigma_{i,\min} \leq \varsigma_i \leq \varsigma_{i,\max} \\ 0, \varsigma_i \leq \varsigma_{i,\min} \end{cases} \quad (12)$$

where  $M(\varsigma_i, V_{com})$  is the gain function, which describes the influence of  $\varsigma_i$  and  $V_{com}$  on  $\Delta K_{pi}^{MM}$ ;  $V' = V_{com} - (V_{com,\min} + V_{com,\max})/2$ ;  $\varsigma' = \varsigma_i - \varsigma_{i,\min}$ ,  $\varsigma_{i,\min}$  and  $\varsigma_{i,\max}$  represent the minimum and maximum values of  $\varsigma_i$ , respectively;  $\Delta K_{pi,0}^{MM}$  is the value of  $\Delta K_{pi}^{MM}$  at the steady state;  $\beta_i$ ,  $l_i$ ,  $\alpha_i$  and  $q_i$  are all adjustable constants.

Moreover, a visualization of the gain function designed by the equations (11) and (12) is given in Fig. 5, where the coordinate values of  $\frac{d\varsigma_i}{dt}$ ,  $\varsigma_i$ ,  $V_{com}$ ,  $\Delta K_{pi}^{GM}$  and  $\Delta K_{pi}^{MM}$  are selected as the respective per-unit values.

*Remark 1:* After the proposed adaptive control strategy is in place, the observation is made. Note that the steady state values of  $J_i$  and  $\Delta K_{pi}$  ( $\varsigma_{i,0} - \varsigma_i$ ) in (5) and (7) are  $J_{i0}$  and zero. As a direct result,  $J_i$  and  $D_i^{AC}$  ( $D_i^{DC}$ ) remain as the original inertia coefficient and frequency (voltage) droop coefficient, respectively. That is, the desired dynamic performance can be guaranteed and the steady state frequency (voltage) droop characteristic is preserved.

## V. SYSTEM STABILITY ANALYSIS AND PARAMETERS SELECTION

The proposed adaptive virtual inertia and virtual governor-gain control strategy can improve the frequency and dc voltage stability of the networked AC/DC MGs by suppressing frequency and dc voltage mutation rate. In order to investigate the influences of inertia and governor-gain on system stability, the small-signal model of the networked AC/DC MGs connected by MTDC is established and its eigenvalue analysis is provided, which guides the design and selection of control parameters.

### A. Small-Signal Modelling of the Networked AC/DC MGs

The small-signal models of the AC MG and the DC MG can be obtained by using similar method proposed in [32] and will not be described in detail here. The equations (5) to (8) describe the dynamic model of the DC-AC IC and the DC-DC IC. By using small signal approximation, (5) to (8) is linearized as

$$\Delta \dot{\mathbf{X}}_{IC} = \mathbf{A}'_{IC-AC} \Delta \mathbf{X}_{AC} + \mathbf{A}'_{IC-DC} \Delta \mathbf{X}_{DC} + \mathbf{A}'_{IC} \Delta \mathbf{X}_{IC} + \mathbf{B}_{IC} \Delta \mathbf{I}_{out}^{ic,dq} + \mathbf{C}_{IC} \Delta \mathbf{d}_b \quad (13)$$

where

$$\begin{aligned} \Delta \mathbf{X}_{IC} &= [\Delta \boldsymbol{\omega}, \Delta \boldsymbol{\psi}, \Delta \mathbf{V}_{ref}, \Delta \mathbf{i}_{dc}, \Delta \mathbf{V}_{com}, \Delta \eta, \Delta \mathbf{V}, \Delta \mathbf{i}_{out}, \Delta \boldsymbol{\beta}]^T, \\ \Delta \mathbf{X}_{AC} &= [\Delta \delta, \Delta \boldsymbol{\omega}_{inv}, \Delta \mathbf{V}_{inv}, \Delta \mathbf{I}_{line}^{ac}, \Delta \mathbf{I}_{load}^{ac}]^T, \\ \Delta \mathbf{X}_{DC} &= [\Delta \mathbf{V}_{dc}, \Delta \mathbf{I}_{line}^{dc}]^T, \Delta \mathbf{d}_b = [\Delta d_{b,1} \cdots \Delta d_{b,I}]^T, \\ \Delta \mathbf{I}_{out}^{ic,dq} &= [\Delta I_{out,1}^{ic,d}, \Delta I_{out,1}^{ic,q}, \dots, \Delta I_{out,I}^{ic,d}, \Delta I_{out,I}^{ic,q}]^T, \end{aligned}$$

$\Delta \boldsymbol{\psi} = \Delta \mathbf{M}_f \mathbf{i}_f$ ,  $\Delta \eta = \int \Delta \mathbf{V}_{com}$ ,  $\Delta \boldsymbol{\beta} = \int \Delta \mathbf{V}_{dc}$ . Matrices  $\mathbf{A}'_{IC-AC}$ ,  $\mathbf{A}'_{IC-DC}$ ,  $\mathbf{A}'_{IC}$ ,  $\mathbf{B}_{IC}$  and  $\mathbf{C}_{IC}$  are given in Appendix.  $\Delta \mathbf{I}_{out}^{ic,dq}$  and  $\Delta \mathbf{d}_b$  represent the small-signal model for the controlled outflow DC-AC IC current and the duty cycle of the switch in the DC-DC IC, respectively.

As described earlier, the small-signal models of real power and reactive power introduced by each DC-AC IC are determined by

$$\begin{aligned} \Delta P_{ic,i}^{pac} &= \frac{k_{pi}^{AC}}{2\pi} \Delta \omega_{m,pu} + \frac{k_{fi}^{AC}}{2\pi} \Delta \delta_{m,pu} + k_{pi}^{AC} \Delta V_{com,pu} \\ &\quad - k_{fi}^{AC} \Delta \eta \\ \Delta Q_{out,i} &= \frac{3\psi_i^{(0)} P_{ic,i}^{pac,(0)}}{2V_{ic,i}^{ac,(0)}} \Delta \omega_i + \frac{3\omega_0 P_{ic,i}^{pac,(0)}}{2V_{ic,i}^{ac,(0)}} \Delta \psi_i + \frac{3\omega_0 \psi_i^{(0)}}{2} \Delta I_{out,i}^{ic,d} \end{aligned} \quad (14)$$

The real power and reactive power flow from each DC-AC IC to AC MG are given as

$$P_{ic,i}^{ac} = V_{ic,i}^{ac} I_{out,i}^{ic,d}, Q_{out,i} = V_{ic,i}^{ac} I_{out,i}^{ic,q} \quad (15)$$

where  $V_{ic,i}^{ac}$  is the voltage magnitude of each DC-AC IC's AC terminal. Hence, the small-signal model for  $\mathbf{I}_{out}^{ic,dq}$  can be written as

$$\Delta \mathbf{I}_{out}^{ic,dq} = \mathbf{C}_{out-AC} \Delta \mathbf{X}_{AC} + \mathbf{C}_{out-IC} \Delta \mathbf{X}_{IC} \quad (16)$$

where matrices  $\mathbf{C}_{out-AC}$  and  $\mathbf{C}_{out-IC}$  are given in Appendix.

According to the model of the DC-DC IC shown in Fig. 4, the average voltage  $e'_i = d_{b,i} V_i$  over a switching period is determined by the output reference value  $V_{ref,i} = d_{b,i} e'_i$ , the small-signal model can be expressed as

$$\Delta \mathbf{d}_b = \mathbf{C}_{db-IC} \Delta \mathbf{X}_{IC} \quad (17)$$

where

$$\begin{aligned} \mathbf{C}_{db-IC} &= [\mathbf{0}, \mathbf{0}, \mathbf{C}_{db,V_{ref}}, \mathbf{0}, \mathbf{0}, \mathbf{0}, \mathbf{C}_{db,V}, \mathbf{0}, \mathbf{0}], \\ \mathbf{C}_{db,V_{ref}} &= \text{diag} \left\{ \left[ \frac{1}{2d_{b,1}^{(0)} V_1^{(0)}} \cdots \frac{1}{2d_{b,I}^{(0)} V_I^{(0)}} \right] \right\}, \\ \mathbf{C}_{db,V} &= \text{diag} \left\{ \left[ \frac{-d_{b,1}^{(0)}}{2V_1^{(0)}} \cdots \frac{-d_{b,I}^{(0)}}{2V_I^{(0)}} \right] \right\}. \end{aligned}$$

By merging (13), (16) and (17), we have the following small-signal state-space equation of the IC section

$$\Delta \dot{\mathbf{X}}_{IC} = \mathbf{A}_{IC-AC} \Delta \mathbf{X}_{AC} + \mathbf{A}_{IC-DC} \Delta \mathbf{X}_{DC} + \mathbf{A}_{IC} \Delta \mathbf{X}_{IC} \quad (18)$$

where

$$\begin{aligned} \mathbf{A}_{IC-AC} &= \mathbf{A}'_{IC-AC} + \mathbf{B}_{IC} \mathbf{C}_{out-AC}, \mathbf{A}_{IC-DC} = \mathbf{A}'_{IC-DC}, \\ \mathbf{A}_{IC} &= \mathbf{A}'_{IC} + \mathbf{B}_{IC} \mathbf{C}_{out-IC} + \mathbf{C}_{IC} \mathbf{C}_{db-IC}. \end{aligned}$$

According to [32], the complete small-signal state-space

model of the AC MG and DC MG is obtained as

$$\begin{aligned} \Delta \dot{\mathbf{X}}_{AC} &= \mathbf{A}'_{AC} \Delta \mathbf{X}_{AC} + \mathbf{B}_{AC} \Delta \mathbf{I}_{in}^{ac} \\ \Delta \dot{\mathbf{X}}_{DC} &= \mathbf{A}'_{DC} \Delta \mathbf{X}_{DC} + \mathbf{B}_{DC} \Delta \mathbf{I}_{out}^{dc} \end{aligned} \quad (19)$$

where matrices  $\mathbf{A}'_{AC}$ ,  $\mathbf{B}_{AC}$ ,  $\mathbf{A}'_{DC}$  and  $\mathbf{B}_{DC}$  are consistent with [32].  $\Delta \mathbf{I}_{in}^{ac} = (\mathbf{D}_{bus-ic}^{ac})^T \mathbf{C}_{TI}^{ic} \Delta \mathbf{I}_{out}^{ic,dq}$ ,  $\Delta \mathbf{I}_{out}^{dc} = (\mathbf{D}_{bus-ic}^{dc})^T \mathbf{C}_{idc} \Delta \mathbf{X}_{IC}$ .  $\mathbf{C}_{TI}^{ic} = \text{diag} \{ [\mathbf{C}_{TI,1}^{ic} \cdots \mathbf{C}_{TI,I}^{ic}] \}$ ,

$$\mathbf{C}_{TI,i}^{ic} = \begin{bmatrix} \cos \theta_i & -\sin \theta_i \\ \sin \theta_i & \cos \theta_i \end{bmatrix}, \mathbf{C}_{idc} = [0, 0, 0, 1, 0, 0, 0, 0].$$

By merging (16) and (19), we have the following small-signal state-space model of the AC MG and DC MG

$$\begin{aligned} \Delta \dot{\mathbf{X}}_{AC} &= \mathbf{A}_{AC} \Delta \mathbf{X}_{AC} + \mathbf{A}_{AC-DC} \Delta \mathbf{X}_{DC} + \mathbf{A}_{AC-IC} \Delta \mathbf{X}_{IC} \\ \Delta \dot{\mathbf{X}}_{DC} &= \mathbf{A}_{DC-AC} \Delta \mathbf{X}_{AC} + \mathbf{A}_{DC} \Delta \mathbf{X}_{DC} + \mathbf{A}_{DC-IC} \Delta \mathbf{X}_{IC} \end{aligned} \quad (20)$$

where

$$\begin{aligned} \mathbf{A}_{AC} &= \mathbf{A}'_{AC} + \mathbf{B}_{AC} (\mathbf{D}_{bus-ic}^{ac})^T \mathbf{C}_{TI}^{ic} \mathbf{C}_{out-AC}, \mathbf{A}_{AC-DC} = \\ \mathbf{A}_{AC-IC} &= \mathbf{B}_{AC} (\mathbf{D}_{bus-ic}^{ac})^T \mathbf{C}_{TI}^{ic} \mathbf{C}_{out-IC}, \mathbf{A}_{DC-AC} = \mathbf{0}, \\ \mathbf{A}_{DC} &= \mathbf{A}'_{DC}, \mathbf{A}_{DC-IC} = \mathbf{B}_{DC} (\mathbf{D}_{bus-ic}^{dc})^T \mathbf{C}_{idc}. \end{aligned}$$

Finally, the small-signal state-space model of the networked AC/DC MGs is derived by integrating (18) and (20)

$$\Delta \dot{\mathbf{X}} = \mathbf{A} \cdot \Delta \mathbf{X} \quad (21)$$

where

$$\begin{aligned} \Delta \mathbf{X} &= [ \Delta \mathbf{X}_{AC} \quad \Delta \mathbf{X}_{DC} \quad \Delta \mathbf{X}_{IC} ]^T, \\ \mathbf{A} &= \begin{bmatrix} \mathbf{A}_{AC} & \mathbf{A}_{AC-DC} & \mathbf{A}_{AC-IC} \\ \mathbf{A}_{DC-AC} & \mathbf{A}_{DC} & \mathbf{A}_{DC-IC} \\ \mathbf{A}_{IC-AC} & \mathbf{A}_{IC-DC} & \mathbf{A}_{IC} \end{bmatrix}. \end{aligned}$$

### B. Small-Signal Stability Analysis and Parameters Selection

Further, we take the networked AC/DC MGs composed of an AC MG and a DC MG as an example to explore the effects of inertia and governor-gain perturbation on the system stability. The parameters and initial conditions of the networked AC/DC MGs are given in Table I in Appendix and the remaining is consistent with [32].

According to the model expressed by (21), the trajectories of the eigenvalues with the virtual inertia coefficients  $J^{AC}$  from 1e-2 to 15 in step of 1e-2 and  $J^{DC}$  from 1e-2 to 30 in step of 5e-2, and the governor-gain coefficients  $\Delta K_{pi}^{GM}$  and  $\Delta K_{pi}^{MM}$  from 1e3 to 5e3 in step of 1e2 are shown in Fig. 6. It can be seen that, the eigenvalues in Fig. 6(a) are very close to the right plane when there is a small virtual inertia  $J^{AC}$ , and the stable state is easily destroyed when the system experiences a disturbance. With the gradual increase of  $J^{AC}$ , the eigenvalues are moving toward the left plane and away from the imaginary axis, which enhances system damping to some extent. However, as  $J^{AC}$  continues to increase, the real parts of the eigenvalues approach to zero, and become positive for  $J^{AC} > 14.9$ , which results in system instability. For the root locus with changing the virtual inertia  $J^{DC}$ , the same effect as changing  $J^{AC}$  can be seen. With the gradual increase of  $J^{DC}$ , the eigenvalues in Fig. 6(b) are moving away from

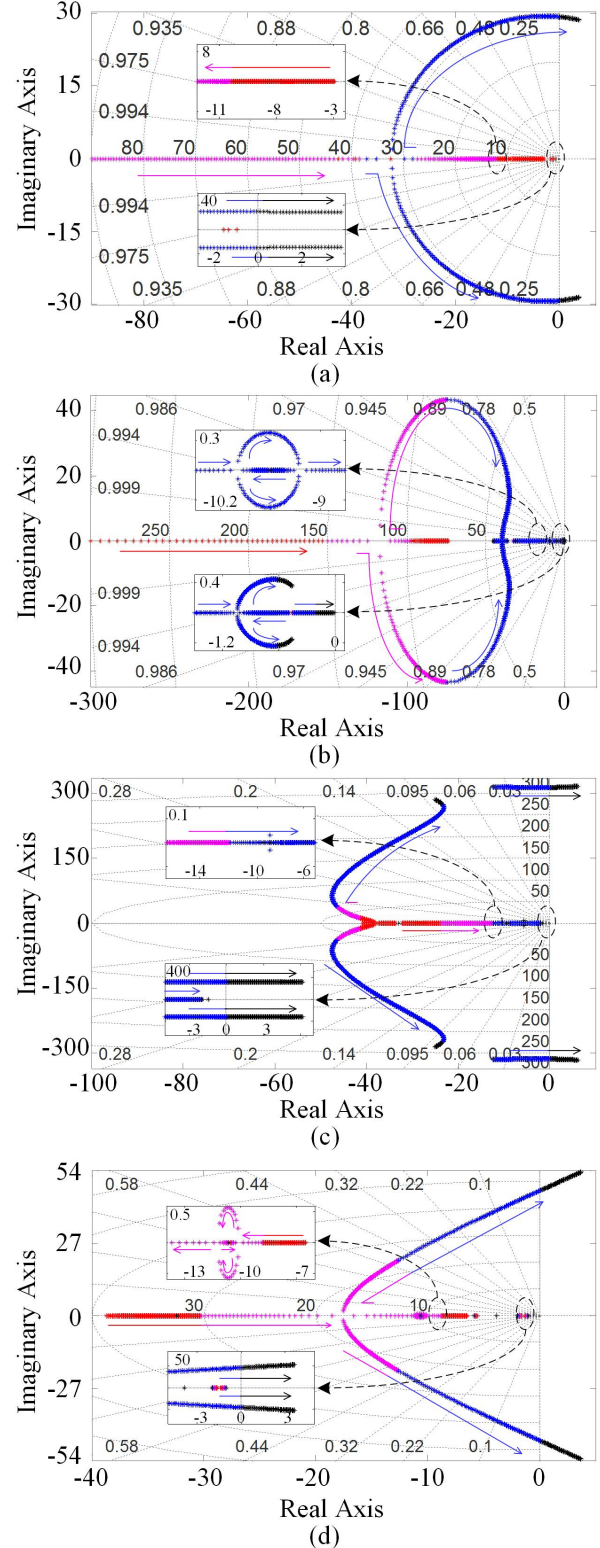


Fig. 6. The root locus with control parameters varying. (a) Varying of  $J^{AC}$ . (b) Varying of  $J^{DC}$ . (c) Varying of  $\Delta K_{pi}^{GM}$ . (d) Varying of  $\Delta K_{pi}^{MM}$ .

the imaginary axis and toward the left plane, which enhances system damping and improves system stability. However, with the further increase of  $J^{DC}$ , the eigenvalues start to move

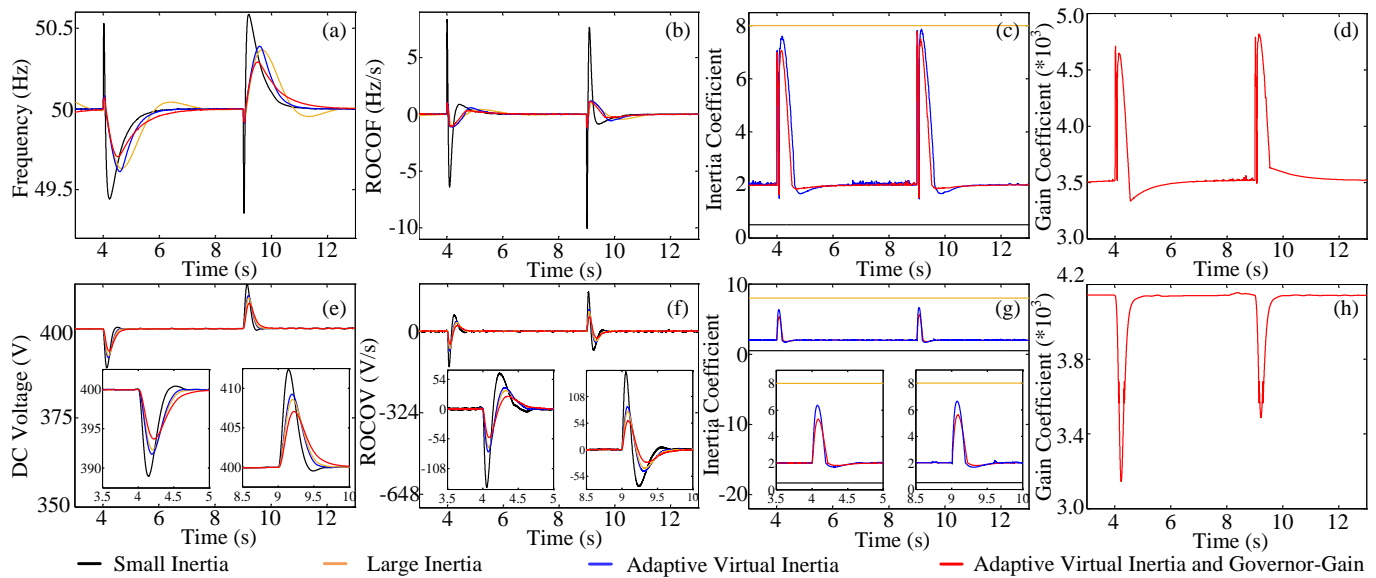


Fig. 7. Effects of inertia and governor-gain response of the proposed control strategy on AC-side and DC-side under load changes. (a) System frequency. (b) ROCOF. (c) Inertia coefficient of DC-AC IC. (d) Governor-gain coefficient of DC-AC IC. (e) DC voltage. (f) ROCOV. (g) Inertia coefficient of DC-DC IC. (h) Governor-gain coefficient of DC-DC IC.

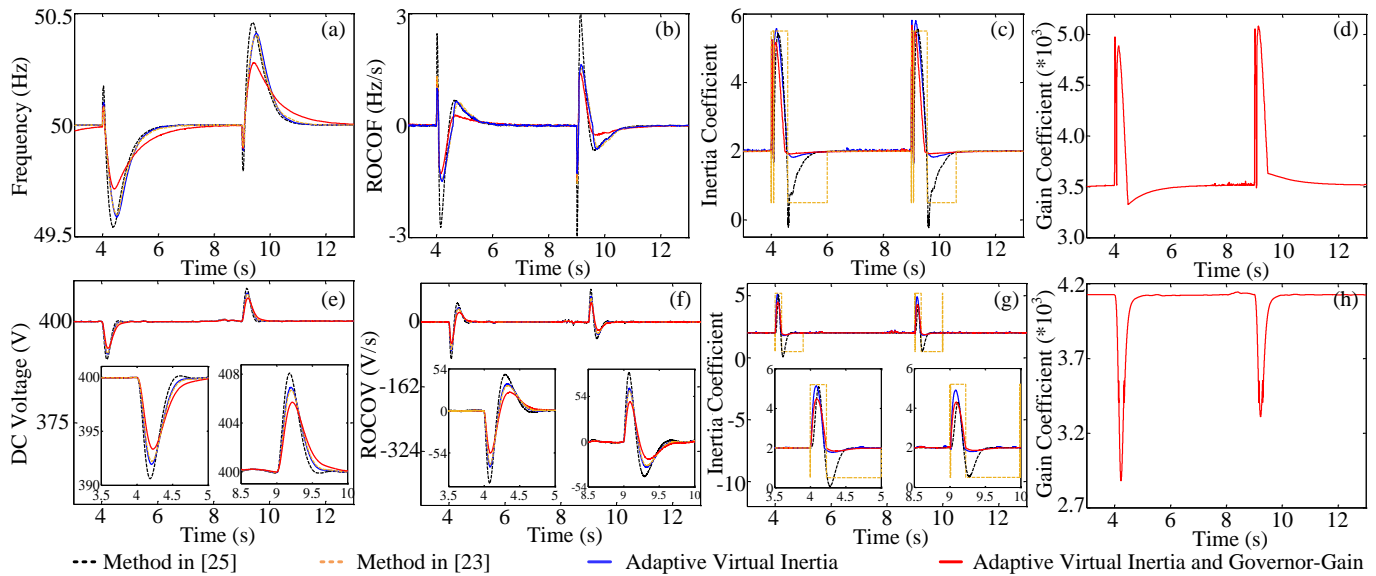


Fig. 8. Comparison among inertia and governor-gain response of the proposed control strategy, method in [23] and method in [25] under load changes. (a) System frequency. (b) ROCOF. (c) Inertia coefficient of DC-AC IC. (d) Governor-gain coefficient of DC-AC IC. (e) DC voltage. (f) ROCOV. (g) Inertia coefficient of DC-DC IC. (h) Governor-gain coefficient of DC-DC IC.

toward the imaginary axis and to the right plane, which is not conducive to the stability of the system. Therefore, the root locus means that the control parameters  $J^{AC}$  and the  $J^{DC}$  should be selected depends on the requirements to system stability, and the physical meaning of this conclusion is also very clear. That is, a small virtual inertia can improve the response speed of the system, but at the cost of loss stability margin; on the other hand, the phase margin of the system has an inverse relationship with the virtual inertia.

Then, the effects of the virtual governor-gain coefficients  $\Delta K_{pi}^{GM}$  of DC-AC IC and the  $\Delta K_{pi}^{MM}$  of DC-DC IC are studied, respectively. As can be observed, the eigenvalues in Fig. 6(c) are moving away from the imaginary axis with

the gradual increase of the  $\Delta K_{pi}^{GM}$ , which enhances system damping. However, with the further increase, the eigenvalues start to move to the right plane for  $\Delta K_{pi}^{GM} > 4890$ , which destroys the stability of the system. In addition, the similar effects of the  $\Delta K_{pi}^{MM}$  and the  $\Delta K_{pi}^{GM}$  can be seen. With the gradual increase of  $\Delta K_{pi}^{MM}$ , the eigenvalues in Fig. 6(d) are moving toward the left plane and away from the imaginary axis, which improves the stability of the system. However, as  $\Delta K_{pi}^{GM}$  further increases, the real parts of eigenvalues start to approach to the right plane for  $\Delta K_{pi}^{MM} > 4760$ , which destabilizes the system. Therefore, the control parameters  $\Delta K_{pi}^{GM}$  and the  $\Delta K_{pi}^{MM}$  should be selected depends on the

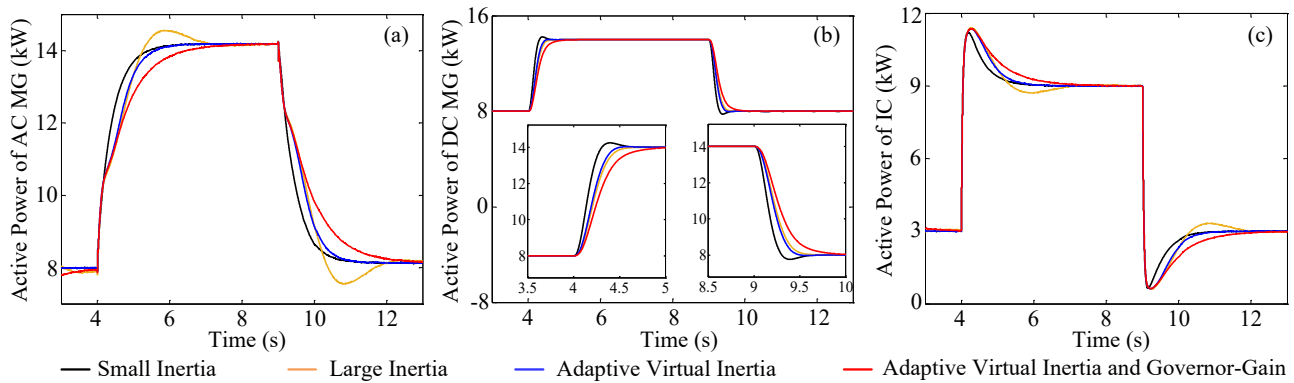


Fig. 9. Effects of inertia and governor-gain response of the proposed control strategy on AC-side and DC-side output power under load changes. (a) AC MG output active power. (b) DC MG output active power. (c) Transferred active power.

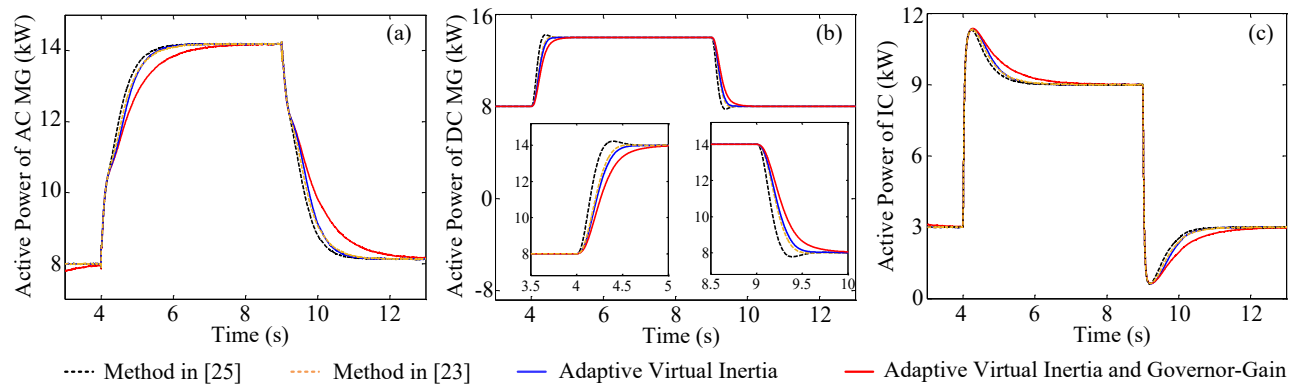


Fig. 10. Comparison of AC-side and DC-side output power response among the proposed control strategy, method in [23] and method in [25] under load changes. (a) AC MG output active power. (b) DC MG output active power. (c) Transferred active power.

requirements to the absorbed power avoiding from exceeding the allowed value, which is consistent with our analysis above.

The stability analysis conducted above provides theoretical guidance for the optimal design of inertia and governor-gain of the actual prototype. In addition, the control parameters that satisfy the stability of the system can also be selected based on linear matrix inequality (LMI). Specifically, for the linear system expressed by (21), the determination of Lyapunov stability can be naturally expressed as the problem of solving Lyapunov inequality, that is,

$$\mathbf{A}^T \mathbf{P} + \mathbf{P} \mathbf{A} < 0 \quad (22)$$

where  $\mathbf{P}$  is a symmetric matrix. By ensuring the existence of positive definite feasible solution  $\mathbf{P}$  for the Lyapunov inequality (22), the selected control parameters satisfy the stability of the system. MATLAB provides the LMI toolbox, which can be solved directly. Interested readers can refer to [33], which will not be detailed here.

## VI. SIMULATION RESULTS

Simulations based on MATLAB/Simulink are performed to evaluate the proposed strategy and the test structure of networked AC/DC MGs consists of an AC MG connected to a DC-AC IC and a DC MG connected to a DC-DC IC. System parameters of the tested MGs are given in Table I in Appendix. The allowable variation of frequency and dc voltage are 49.5

Hz  $\leq f \leq 50.5$  Hz and  $390\text{V} \leq V_{dc} \leq 410\text{V}$ , respectively. The loads, connected to the two subsystems, are switched between “light” and “heavy” condition to verify the effectiveness of the control strategy proposed in this paper. At first, the AC/DC MGs operates in the steady state under light load. At  $t=4\text{s}$ , the load in the AC-side is switched from light to heavy. At  $t=9\text{s}$ , when the MG reaches the steady state, the load in the AC-side is restored to the initial configuration.

### A. Performance of the Proposed Control Strategy

This paper is dedicated to improving the dynamic stability of frequency and dc voltage when AC-side and/or DC-side load change. With the same scenario adopted, six IC control strategies are compared and verified. For the strategy I, the virtual inertia is set as a small constant ( $J_0=0.5$ ) which implies the conventional droop control. For the strategy II, the virtual inertia is set as a large constant ( $J_0=8$ ) which represents the conventional VSG control. For the strategy III and the strategy IV proposed in this paper, the parameter is listed in Appendix. For the strategy V proposed in [25], the main parameters are set as  $J_0=2$ ,  $k_{ac}=0.82$  (0.07),  $k_{dc}=0.011$  (0.008). For the strategy VI proposed in [23], the main parameters are set as  $J_0=2$ ,  $J_{\max}^{AC}=5.5$  (7.2),  $J_{\min}^{AC}=0.5$ ,  $J_{\max}^{DC}=5.2$  (3.65),  $J_{\min}^{DC}=0.5$ .

Fig. 7 depicts the waves of frequency/DC voltage, RO-COF/ROCOV, inertia and governor-gain with adopting the

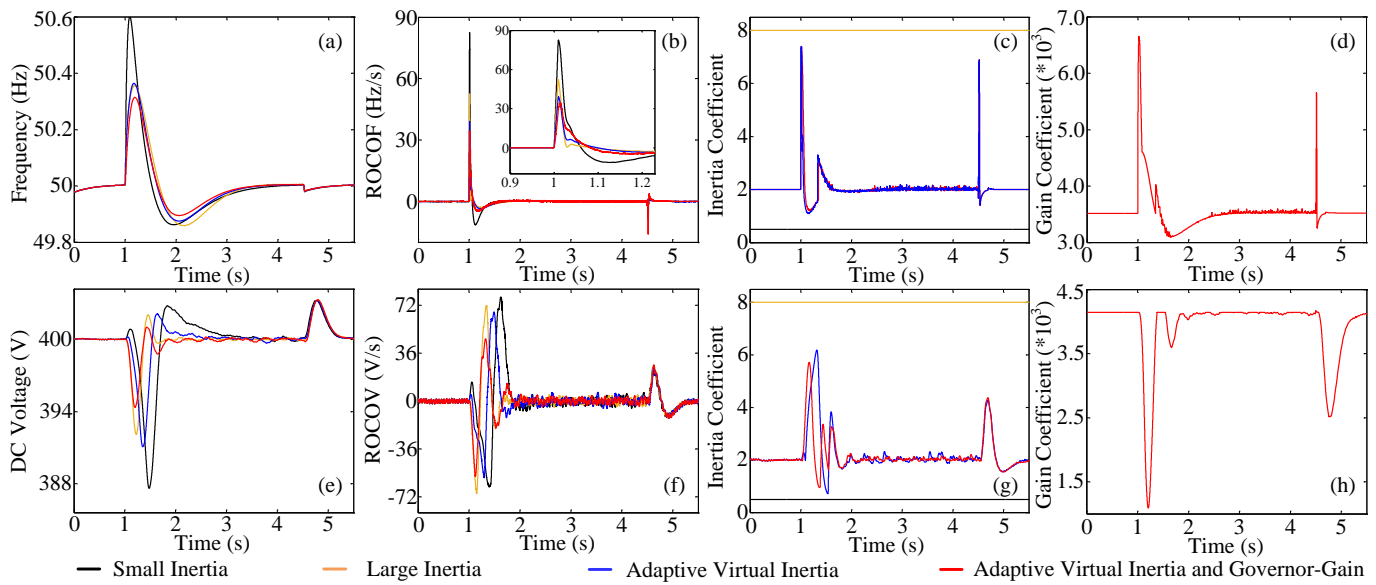


Fig. 11. Effects of inertia and governor-gain response of the proposed control strategy on AC-side and DC-side under connection and disconnection switching between AC MG and DC MG. (a) System frequency. (b) ROCOF. (c) Inertia coefficient of DC-AC IC. (d) Governor-gain coefficient of DC-AC IC. (e) DC voltage. (f) ROCOV. (g) Inertia coefficient of DC-DC IC. (h) Governor-gain coefficient of DC-DC IC.

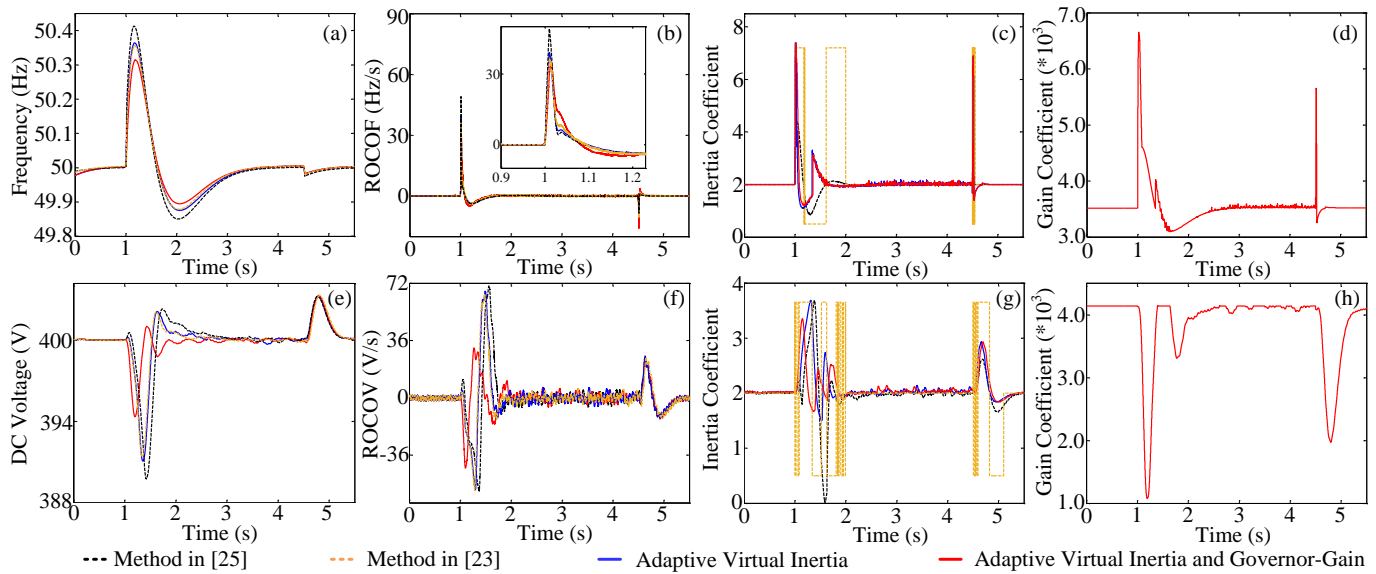


Fig. 12. Comparison among inertia and governor-gain response of the proposed control strategy, method in [23] and method in [25] under connection and disconnection switching between AC MG and DC MG. (a) System frequency. (b) ROCOF. (c) Inertia coefficient of DC-AC IC. (d) Governor-gain coefficient of DC-AC IC. (e) DC voltage. (f) ROCOV. (g) Inertia coefficient of DC-DC IC. (h) Governor-gain coefficient of DC-DC IC.

strategy III and the strategy IV proposed in this paper and the conventional droop control and the VSG control. As observed, the control effects of these four different strategies are obviously different. The rebound speed is extremely fast with small constant inertia (see Fig. 7(a) and (e)), whereas the nadir of arrested frequency/DC voltage even exceeds the normal operating range and ROCOF/ROCOV is very large. With large constant inertia, the nadir of arrested frequency/DC voltage and ROCOF/ROCOV are higher and lower than the small inertia constant, whereas the rebound speed is extremely slow and the oscillation exists. When applying the proposed adaptive virtual inertial control, although the nadir of arrested frequency/DC voltage and ROCOF/ROCOV are slightly lower

and larger than the large constant inertia, the oscillation and the dynamic performance of the system are eliminated and improved. Comparing with these four control strategies, the overall performance of applying the proposed adaptive virtual inertial and virtual governor-gain control is the best. That is, the nadir of frequency/DC voltage and ROCOF/ROCOV are the highest and the smallest, and the rebound speed is similar to the small constant inertia. This can also be explained by the curves of the inertia and the governor-gain as shown in Fig. 7(c) and (g) and Fig. 7(d) and (h). A relatively large inertia and governor-gain are provided at the beginning of the disturbance, and a relatively small inertia and governor-gain are provided during the “rebound period”. Following, we

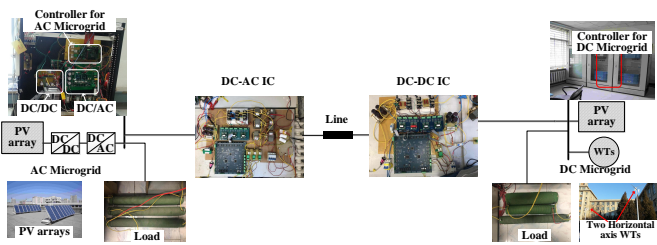


Fig. 13. The tested networked AC/DC MGs

further compare the proposed method (Strategy III and IV) with existing adaptive methods recently published in [23] and [25]. The results are shown in Fig. 8. It is noted that the control effects vary greatly in the the nadir of frequency/DC voltage, ROCOF/ROCOV and the rebound speed. Among them, the disturbed frequency/DC voltage with the method in [25] can be restored to the steady state value as soon as possible, whereas the nadir values and ROCOF/ROCOV are lower and larger than the other three control strategies, respectively; the nadir of frequency/DC voltage and ROCOF/ROCOV with the method in [23] are similar to that of the adaptive virtual inertial control proposed in this paper, whereas the rebound speed with the latter is faster; the control effect of the strategy IV is the best. Not only the nadir values and ROCOF/ROCOV are the highest and the smallest, but also the rebound speed is similar to the other three control strategies. The above description can be well explained by the curves of the inertia and the governor-gain shown in Fig. 8(c), (d), (g) and (h). For the method in [25], the oversize value of compensation coefficient  $k_{ac}$  cannot be acquired on account of the limitation of the range of inertia, which hinders the adjustment of inertia in other cases. For the method in [23], the virtual inertia is adjusted to the maximum at the beginning of the disturbance, maintained until the rebound period and then switched to the minimum until the steady state interval, so that the risk of the system being disturbed is increased. For the proposed strategy in this paper, the virtual inertia and the governor-gain are adjusted to the maximum at the beginning of the disturbance and then decreased gradually and finally returned to the stable value, so that the nadir values, ROCOF/ROCOV and the rebound speed are improved very well.

### B. Proper Power Sharing

In addition to the stability of dynamic frequency and dc voltage, proper power sharing is also a basic control task for ICs. For the convenience of result analysis, the rated power of DC MG and AC MG is set to be the same as the 20 kW. Therefore, as long as the two MGs have the same steady state output power under different load conditions, it can prove that the proper power sharing among the networked AC/DC MGs is realized. From Fig. 9 and Fig. 10, the output power of the DC MG is about 8kw from  $t=0s$  to  $t=4s$ , which is equal to the output value of the AC MG; from  $t=4s$  to  $t=9s$ , the output power of the DC MG is about 14kw, and so is the AC MG; finally, the output power of the two MGs is still roughly equal. Therefore, proper power sharing among

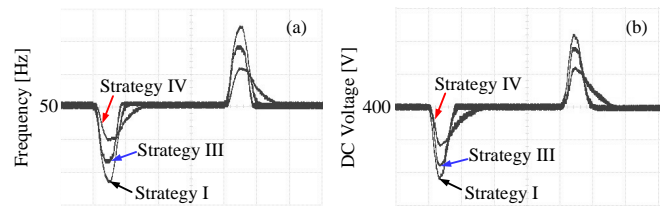


Fig. 14. Comparison of experimental results of frequency and dc voltage response among strategy I (small inertia), strategy III and strategy IV proposed in this paper. (a) System frequency (scales: 0.2Hz/div, 2s/div). (b) DC voltage (scales: 5V/div, 2s/div)).

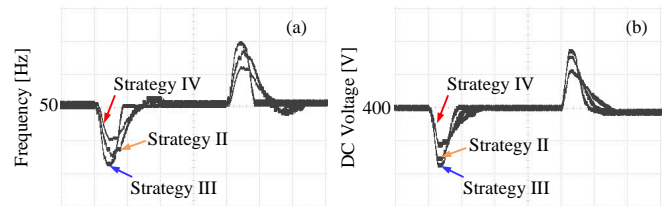


Fig. 15. Comparison of experimental results of frequency and dc voltage response among strategy II (large inertia), strategy III and strategy IV proposed in this paper. (a) System frequency (scales: 0.2Hz/div, 2s/div). (b) DC voltage (scales: 5V/div, 2s/div)).

the test AC/DC MGs can be achieved. As for the dynamic response of the power, it can be seen from Fig. 9 that there exists oscillation in the output power of AC MG with the application of large constant inertial control. However, when applying the proposed adaptive virtual inertial control, not only can power oscillation be eliminated, but also the output power of AC MG and DC MG can be smoothed. In addition, as depicted in Fig. 9(a) and Fig. 9(b), the smoothest output power of AC MG and DC MG can be obtained by applying the proposed adaptive virtual inertial and virtual governor-gain control, which means that it has excellent power oscillation damping function. On the other hand, as shown in Fig. 9(c), the IC transferred active power by the proposed control strategy works best, that is, not only is there no power oscillation, but also a large power can be quickly supplied to suppress ROCOF and/or ROCOV at the moment of disturbance.

Comparison of the proposed method (strategy III and IV) with the existing adaptive methods in [23] and [25] is also considered. The corresponding results are shown in Fig. 10. As observed, excellent power oscillation damping is achieved using these methods. Meanwhile, the dynamic response of the output power is different. Specifically, with the method in [25], the output power of MGs is faster than others when the load changes, whereas the IC transferred active power is slowly supplied; the response of output power with the method in [23] is similar to that of adaptive virtual inertial control proposed in this paper. With the proposed method, the smoothest output power of AC MG and DC MG, and the fastest IC transferred active power can be obtained at the same time.

### C. Performance under Connection and Disconnection Switching

In order to further illustrate the performance of the proposed control strategy, this section simulates the connection and

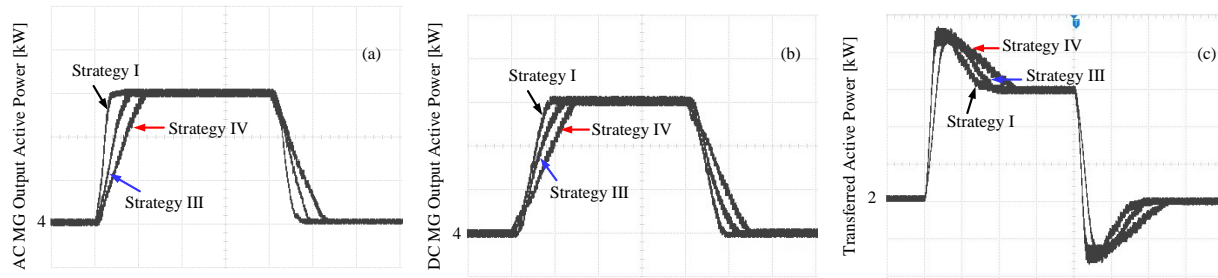


Fig. 16. Comparison of experimental results of AC-side and DC-side output power response among strategy I (small inertia control), strategy III and strategy IV proposed in this paper. (c) AC MG output active power (scales: 1kW/div, 2s/div). (d) DC MG output active power (scales: 1kW/div, 2s/div). (e) Transferred active power (scales: 1kW/div, 2s/div).

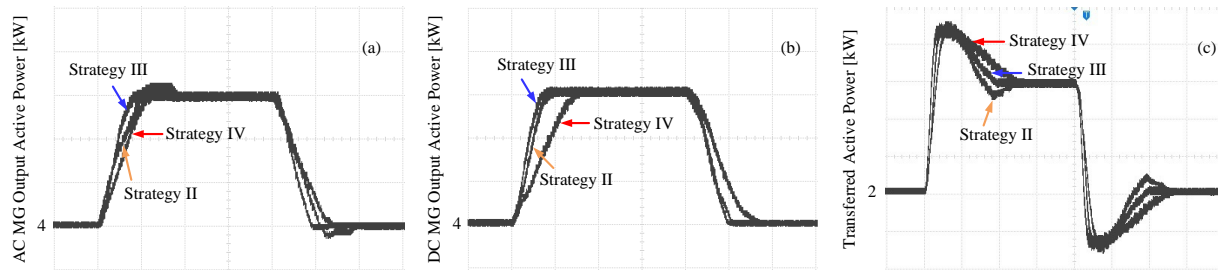


Fig. 17. Comparison of experimental results of AC-side and DC-side output power response among strategy II (large inertia control), strategy III and strategy IV proposed in this paper. (c) AC MG output active power (scales: 1kW/div, 2s/div). (d) DC MG output active power (scales: 1kW/div, 2s/div). (e) Transferred active power (scales: 1kW/div, 2s/div).

disconnection switching between the AC MG connected to the DC-AC IC and the DC MG connected to the DC-DC IC.

As shown in Fig. 11, the overshoot of frequency and dc voltage is extremely large with small constant inertia (exceeding the normal operating range of frequency and dc voltage). For large constant inertia control, although the overshoot becomes smaller, the oscillation degrades the dynamic performance of the system. As for the simulation results of applying proposed adaptive virtual inertial control, not only can frequency and dc voltage change steadily in the process of transient regulation (from  $t=1s$  to  $t=4.5s$ ), but also ROCOF and ROCOV are lower than those using large constant inertial control. And when applying adaptive virtual inertial and virtual governor-gain control, not only the overshoot of frequency and dc voltage is the smallest, but also the nadirs of arrested frequency and dc voltage are the highest. On the other hand, when the switching is disconnected ( $t=4.5s$ ), the dynamic response of frequency and dc voltage with these four IC control strategies is similar to each other, which is due to the fact that the inertia of both the tested AC MG and DC MG is fixed.

Fig. 12 further demonstrates the performance advantages over existing adaptive methods. Among them, the overshoot of frequency and dc voltage with the method in [25] is larger than the other three control strategies (see Fig. 12(a) and Fig. 12(e)). The control performance with the method in [23] is similar to that of the adaptive virtual inertial control and the best control performance can be obtained with proposed adaptive virtual inertial and virtual governor-gain control method. Therefore, the results show the advantage of the proposed control strategy.

## VII. EXPERIMENTAL RESULTS

A scaled-down networked AC/DC MGs shown in Fig. 13 is built to verify the proposed method, where a DC-AC IC and a DC-DC IC are adopted to interconnect the AC and DC MGs. The ICs are controlled by digital signal processors (TMS320F28335) and the switching frequency is 19.2kHz. The AC MG consists of 10 kW PV arrays, while the DC MG consists of 5 kW PV arrays and 5 kW wind turbines (WTs). The loads that switch between “light” and “heavy” condition are considered for the MGs. At  $t=4s$ , the load in the AC MG is switched from light load to heavy load. At  $t=12s$ , the load in the AC MG is restored to the initial value. The system parameters are listed in Table II in Appendix.

To verify the effectiveness, strategy I and strategy II (small and large inertia) used in the simulation are also applied here to compare with the proposed strategy by changing the load. The results are shown in Fig. 14 and Fig. 15. As observed, the rebound speed is the fastest with the small inertia, whereas the nadirs of arrested frequency and dc voltage almost exceed the normal frequency and dc voltage operating range (49.5Hz~50.5Hz, 390V~410V). With the large inertia, the nadirs of arrested frequency and dc voltage are higher than the small inertial control, whereas the rebound speed is the slowest and the oscillation exists. When applying the proposed adaptive virtual inertial control, although the nadirs of arrested frequency and dc voltage are slightly lower than the large constant inertia control, the oscillation and the rebound speed of the system are eliminated and improved. While for the proposed adaptive virtual inertial and virtual governor-gain control, not only the nadirs of arrested frequency and dc

voltage are the highest, but also the rebound speed is similar to the small constant inertia control.

Furthermore, Fig. 16 and Fig. 17 present the experimental results of AC-side and DC-side output power response under load changes. On the one hand, it can be found that the two MGs can share the load as expected with these four control strategies. That is, the output power (about 4 kW) of the AC MG is approximately equal to that of the DC MG from  $t=0s$  to  $t=4s$ ; from  $t=4s$  to  $t=12s$ , the output power of the AC MG and the DC MG is about 7kw; finally, the equal output power of the two MGs is still maintained. On the other hand, it can be observed that the application of the large constant inertia control leads to the output power oscillation. With the proposed adaptive virtual inertial control, the output power oscillation disappears and is replaced by the gentle output power. And when applying the proposed adaptive virtual inertial and virtual governor-gain control, the smoothest output power of AC MG and DC MG can be observed. In addition, as depicted in Fig. 16(c) and Fig. 17(c), a large active power transferred by IC is quickly supplied when the load changes abruptly, which further proves the effectiveness of the proposed control method.

### VIII. CONCLUSION

This paper proposes a power management approach that can simultaneously enhance the frequency and dc voltage stability of the networked AC/DC MGs while keeping proper power sharing. To realize the objective, the control strategy based on synchronverter and VDCM with the power sharing controller, adaptive virtual inertia regulator and virtual governor has been developed in this paper. Also, the clear mathematical expressions of adaptive virtual inertia and virtual governor-gain determined by the frequency and/or dc voltage, virtual rotor speed, and ROCOF and/or ROCOV are constructed. In addition, the small-signal stability analysis of the networked AC/DC MGs with the proposed control strategy is proposed to guide the design and selection of control parameters. Finally, Simulation and experimental results have been given to verify the performance of proposed control strategy.

Currently, although adaptive virtual inertia and virtual governor-gain control strategy is proposed, the optimal values of these parameters are not discussed and cannot be guaranteed by this approach. Therefore, the optimal adaptive virtual inertia and virtual governor-gain control will be explored in our future work. Another future direction is concerned with the participation in the ancillary service market, which means that how each MG or the networked AC and DC MGs can provide virtual inertia service for the system via ancillary service market.

### APPENDIX

The matrices of equation (13).

$$\begin{aligned} A'_{IC-AC} &= \begin{bmatrix} C' & 0 \\ 0 & 0 \end{bmatrix}, A'_{IC} = \begin{bmatrix} E'_1 & E'_2 \\ 0 & E'_3 \end{bmatrix}, \\ A'_{IC-DC} &= [0, D'_1, 0, D'_2]^T, \\ B_{IC} &= \begin{bmatrix} B'_{IC} \\ 0 \end{bmatrix}, C_{IC} = \begin{bmatrix} 0 \\ C'_{IC} \\ 0 \end{bmatrix}, \end{aligned}$$

$$\begin{aligned} C' &= \begin{bmatrix} A_{\omega\delta} & A_{\omega\omega_{inv}} & 0 \\ A_{\psi\delta} & 0 & A_{\psi V_{inv}} \\ 0 & 0 & 0 \\ 0 & 0 & 0 \\ A_{V_{com}\delta} & A_{V_{com}\omega_{inv}} & 0 \end{bmatrix}, \\ D'_1 &= \begin{bmatrix} A_{V_{ref}V_{dc}} & 0 \\ A_{i_{dc}V_{dc}} & 0 \end{bmatrix}, D'_2 = \begin{bmatrix} A_{VV_{dc}} & 0 \\ 0 & 0 \\ A_{\beta V_{dc}} & 0 \end{bmatrix}, \\ E'_1 &= \begin{bmatrix} A_{\omega} & A_{\omega\psi} & 0 & 0 \\ A_{\psi\omega} & A_{\psi} & 0 & 0 \\ 0 & 0 & A_{V_{ref}} & A_{V_{ref}i_{dc}} \\ 0 & 0 & 0 & A_{i_{dc}} \end{bmatrix}, \\ E'_2 &= \begin{bmatrix} A_{\omega V_{com}} & A_{\omega\eta} & 0 & 0 & 0 \\ 0 & 0 & 0 & 0 & 0 \\ A_{V_{ref}V_{com}} & A_{V_{ref}\eta} & 0 & 0 & A_{V_{ref}\beta} \\ 0 & 0 & A_{i_{dc}V} & 0 & 0 \end{bmatrix}, \\ E'_3 &= \begin{bmatrix} A_{V_{com}} & A_{V_{com}\eta} & 0 & A_{V_{com}i_{out}} & 0 \\ 1 & 0 & 0 & 0 & 0 \\ A_{VV_{com}} & A_{V\eta} & A_V & A_{Vi_{out}} & A_{V\beta} \\ A_{i_{out}V_{com}} & 0 & A_{i_{out}V} & A_{i_{out}} & 0 \\ 0 & 0 & 0 & 0 & 0 \end{bmatrix}, \\ B'_{IC} &= \begin{bmatrix} 0 & B_{\omega I_{out}^{ic,dq}} \\ B_{\psi I_{out}^{ic,dq}} & 0 \end{bmatrix}, C'_{IC} = \begin{bmatrix} B_{V_{ref}d_b} \\ B_{i_{dc}d_b} \end{bmatrix}, \\ A_{\omega\delta} &= \text{diag} \left\{ \frac{k_i^{AC}}{J_i^{AC} \pi \omega_0} \right\}, A_{\omega_{inv}} = \text{diag} \left\{ \frac{k_i^{AC} - \Delta K_{pi}}{J_i^{AC} \pi \omega_0} \right\}, \\ A_{\omega} &= \text{diag} \left\{ \frac{-D_i^{AC}}{J_i^{AC}} \right\}, A_{\omega\psi} = \text{diag} \left\{ \frac{3P_{ic,i}^{ac,(0)}}{2J_i^{AC} V_{ic,i}^{ac,(0)}} \right\}, \\ A_{\omega V_{com}} &= \text{diag} \left\{ \frac{-k_i^{AC}}{50J_i^{AC} \omega_0} \right\}, A_{\omega\eta} = \text{diag} \left\{ \frac{-k_i^{AC}}{50J_i^{AC} \omega_0} \right\}, \\ B_{\omega I_{out}^{ic,dq}} &= \text{diag} \left\{ \begin{bmatrix} 0 & -3\psi_i^{(0)} \\ -3\omega_0\psi_i^{(0)} & 0 \end{bmatrix} \right\}, C_{TV,i}^{ic} = [\cos \theta_i, \sin \theta_i], \\ B_{\psi I_{out}^{ic,dq}} &= \text{diag} \left\{ \begin{bmatrix} -3\omega_0\psi_i^{(0)} & 0 \\ 2V_{ic,i}^{ac,(0)} & 0 \end{bmatrix} \right\}, C_{\psi_i V_{out,i}} = -\frac{F_i}{K_i}, \\ A_{\psi\delta} &= \text{diag} \left\{ C_{\psi_i V_{out,i}} C_{TV,i}^{ic} D_{bus-ic}^{ac} C_{V_{ac} \delta_{i,m}} \right\}, \\ A_{\psi V_{inv}} &= \text{diag} \left\{ C_{\psi_i V_{out,i}} C_{TV,i}^{ic} D_{bus-ic}^{ac} C_{TV,i,m}^{ac} \right\}, \\ C_{TV,i,m}^{ac} &= [\cos \delta_m^{(0)}, \sin \delta_m^{(0)}]^T, \\ C_{V_{bus}^{ac} \delta_{i,m}} &= [-V_{inv,m}^{(0)} \sin \delta_m^{(0)}, V_{inv,m}^{(0)} \cos \delta_m^{(0)}]^T, \\ A_{\psi\omega} &= \text{diag} \left\{ \frac{3P_{ic,i}^{ac,(0)} \psi_i^{(0)}}{2K_i V_{ic,i}^{ac,(0)}} \right\}, A_{\psi} = \text{diag} \left\{ \frac{3P_{ic,i}^{ac,(0)} \omega_0}{2K_i V_{ic,i}^{ac,(0)}} \right\}, \\ A_{V_{ref}V_{dc}} &= \text{diag} \left\{ \frac{-k_{P_i}^{DC} + \Delta K_{pi}}{10J_i^{DC} V_{ref,i}^{(0)}} \right\}, A_{V_{ref}} = \text{diag} \left\{ \frac{-D_i^{DC}}{J_i^{DC}} \right\}, \\ A_{V_{ref}i_{dc}} &= \text{diag} \left\{ \frac{d_{b,i}^{(0)}}{J_i^{DC}} \right\}, A_{V_{ref}\eta} = \text{diag} \left\{ \frac{k_{P_i}^{DC}}{50J_i^{DC} V_{ref,i}^{(0)}} \right\}, \\ A_{V_{ref}V_{com}} &= \text{diag} \left\{ \frac{k_{P_i}^{DC}}{50J_i^{DC} V_{ref,i}^{(0)}} \right\}, A_{i_{dc}} = \text{diag} \left\{ \frac{-r_{dc,i}}{L_{dc,i}} \right\}, \\ A_{i_{dc}V_{dc}} &= \text{diag} \left\{ \frac{1}{L_{dc,i}} \right\}, A_{V_{ref}\beta} = \text{diag} \left\{ \frac{-k_{P_i}^{DC}}{10J_i^{DC} V_{ref,i}^{(0)}} \right\}, \\ B_{V_{ref}d_b} &= \text{diag} \left\{ \frac{-P_{ic,i}^{dc,0}}{J_i^{DC} V_{ic,i}^{dc,0}} \right\}, A_{i_{dc}V} = \text{diag} \left\{ \frac{-d_{b,i}^{(0)}}{L_{dc,i}} \right\}, \\ B_{i_{dc}d_b} &= \text{diag} \left\{ \frac{-V_i^{(0)}}{L_{dc,i}} \right\}, A_{V_{com}\delta} = \frac{k_{P_i}^{AC}}{\pi C_{V1} V_{com}^{(0)}}, \\ A_{V_{com}\omega_{inv}} &= \frac{k_{P_i}^{AC}}{\pi C_{V1} V_{com}^{(0)}}, A_{V_{com}} = \frac{-k_{P_i}^{AC} V_{com}^{(0)} - 50P_{ic,i}^{ac,(0)}}{50C_{V1} (V_{com}^{(0)})^2}, \\ A_{V_{com}\eta} &= \frac{-k_{P_i}^{AC}}{50C_{V1} V_{com}^{(0)}}, A_{VV_{dc}} = \text{diag} \left\{ \frac{k_{P_i}^{DC}}{10C_i^{DC} V_i^{(0)}} \right\}, \end{aligned}$$

$$\mathbf{A}_{V_{com}i_{out}} = \frac{1}{C_{V1}}, \mathbf{A}_{V_{V_{com}}} = \text{diag} \left\{ \frac{-k_{P_i}^{DC}}{50C_i^{DC}C_{V_i}^{(0)}} \right\},$$

$$\mathbf{A}_{V_{\eta}} = \text{diag} \left\{ \frac{-k_{I_i}^{DC}}{50C_i^{DC}C_{V_i}^{(0)}} \right\}, \mathbf{A}_{V} = \text{diag} \left\{ \frac{-P_{ic,i}^{dc,0}}{C_i^{DC}(V_i^{(0)})^2} \right\},$$

$$\mathbf{A}_{V_{i_{out}}} = \text{diag} \left\{ \frac{-1}{C_i^{DC}} \right\}, \mathbf{A}_{V_{\beta}} = \text{diag} \left\{ \frac{k_{I_i}^{DC}}{10C_i^{DC}C_{V_i}^{(0)}} \right\},$$

$$\mathbf{A}_{i_{out}V_{com}} = \text{diag} \left\{ \frac{-1}{L_{line,i}^{MTDC}} \right\}, \mathbf{A}_{i_{out}V} = \text{diag} \left\{ \frac{1}{L_{line,i}^{MTDC}} \right\},$$

$$\mathbf{A}_{i_{out}} = \text{diag} \left\{ \frac{-R_{line,i}^{MTDC}}{L_{line,i}^{MTDC}} \right\}, \mathbf{A}_{\beta V_{dc}} = \text{diag} \{ [1 \dots 1] \}.$$

The matrices of equation (16).

$$\mathbf{C}_{out-AC} = \left[ \mathbf{C}_{I_{out}^{ic,dq}\delta}, \mathbf{C}_{I_{out}^{ic,dq}\omega_{inv}}, \mathbf{C}_{I_{out}^{ic,dq}V_{inv}}, \mathbf{0} \right],$$

$$\mathbf{C}_{out-IC} = \left[ \mathbf{C}_{I_{out}^{ic,dq}\omega}, \mathbf{C}_{I_{out}^{ic,dq}\psi}, \mathbf{0}, \mathbf{C}_{I_{out}^{ic,dq}V_{com}}, \mathbf{C}_{I_{out}^{ic,dq}\eta}, \mathbf{0} \right],$$

$$\mathbf{C}_{I_{out}^{ic,dq}R} = \text{diag} \left\{ \left[ \begin{array}{cc} \mathbf{C}_{I_{out,i}^{ic,d}R} & \mathbf{C}_{I_{out,i}^{ic,q}R} \end{array} \right] \right\},$$

$$\mathbf{R} = [\delta, \omega_{inv}, V_{inv}, V_{com}, \eta, \omega, \psi],$$

$$\mathbf{C}_{I_{out,i}^{ic,dq}\omega} = \left[ \begin{array}{c} 0, \frac{-3P_{ic,i}^{ac,(0)}\psi_i^{(0)}}{2V_{ic,i}^{ac,(0)}} \end{array} \right], \mathbf{C}_{I_{out,i}^{ic,dq}\psi} = \left[ \begin{array}{c} 0, \frac{-3P_{ic,i}^{ac,(0)}\omega_0}{2V_{ic,i}^{ac,(0)}} \end{array} \right].$$

$$C_{I_{out,i}^{ic,d}\delta} = \frac{k_{I_i}^{AC}}{\pi V_{ic,i}^{ac,(0)}} - \frac{P_{ic,i}^{ac,(0)}C_{TV,i}^{ic}D_{bus-ic}^{ac}C_{V_{bus}^{ac}}\delta_{i,m}}{(V_{ic,i}^{ac,(0)})^2},$$

$$C_{I_{out,i}^{ic,q}\delta} = \frac{-3\omega_0\psi_i^{(0)}}{2V_{ic,i}^{ac,(0)}}C_{I_{out,i}^{ic,d}\delta} - \frac{Q_{out,i}^{(0)}C_{TV,i}^{ic}D_{bus-ic}^{ac}C_{V_{bus}^{ac}}\delta_{i,m}}{(V_{ic,i}^{ac,(0)})^2},$$

$$C_{I_{out,i}^{ic,q}\omega_{inv}} = \frac{k_{I_i}^{AC}}{\pi V_{ic,i}^{ac,(0)}}, C_{I_{out,i}^{ic,q}\omega_{inv}} = \frac{-3\omega_0\psi_i^{(0)}}{2V_{ic,i}^{ac,(0)}}C_{I_{out,i}^{ic,d}\omega_{inv}},$$

$$C_{I_{out,i}^{ic,d}V_{inv}} = \frac{-P_{ic,i}^{ac,(0)}C_{TV,i}^{ic}D_{bus-ic}^{ac}C_{TV,m}^{ac}}{(V_{ic,i}^{ac,(0)})^2},$$

$$C_{I_{out,i}^{ic,q}V_{inv}} = \frac{-3\omega_0\psi_i^{(0)}}{2V_{ic,i}^{ac,(0)}}C_{I_{out,i}^{ic,d}V_{inv}} - \frac{Q_{out,i}^{(0)}C_{TV,i}^{ic}D_{bus-ic}^{ac}C_{TV,m}^{ac}}{(V_{ic,i}^{ac,(0)})^2},$$

$$C_{I_{out,i}^{ic,d}V_{com}} = \frac{-k_{I_i}^{AC}}{50V_{ic,i}^{ac,(0)}}, C_{I_{out,i}^{ic,q}V_{com}} = \frac{-3\omega_0\psi_i^{(0)}}{2V_{ic,i}^{ac,(0)}}C_{I_{out,i}^{ic,d}V_{com}},$$

$$C_{I_{out,i}^{ic,d}\eta} = \frac{-k_{I_i}^{AC}}{50V_{ic,i}^{ac,(0)}}, C_{I_{out,i}^{ic,q}\eta} = \frac{-3\omega_0\psi_i^{(0)}}{2V_{ic,i}^{ac,(0)}}C_{I_{out,i}^{ic,d}\eta}.$$

TABLE I  
SIMULATION SYSTEM PARAMETERS

Items	Parameters & Values
AC MG	$f_0 = 50\text{Hz}$ , $P_{ac,load} = 11\text{kW(Light)}$ $P_{ac,load} = 23\text{kW(Heavy)}$
DC MG	$V_{dc,0} = 400\text{V}$ , $P_{dc,load} = 5\text{kW}$
DC-AC IC	$V_{com,ref} = 700\text{V}$ , $V_{out,ref} = 311\text{V}$ , $K = 7.1$ $L = 6\text{mH}$ , $L_f = 3\text{mH}$ , $C_f = 500\mu\text{F}$ , $F = 321$ $C_{V1} = 2\text{mF}$ , $D^{AC} = 22$ , $k_P^{AC} = 5$ , $k_I^{AC} = 205$
DC-DC IC	$L_{dc} = 0.25\text{mH}$ , $r_{dc} = 0.05\Omega$ , $V_0 = 700\text{V}$ $D^{DC} = 80$ , $k_P^{DC} = 5.5$ , $k_I^{DC} = 205.3$ $k_P^{db} = 3.8$ , $k_I^{db} = 186.5$ , $C^{DC} = 3.2\text{mF}$
$J$	$J_0 = 2$ , $J_{max} = 8$ , $J_{min} = 0.5$
$\Delta K_p$	$\Delta K_{p,0}^{GM} = 2000$ , $\Delta K_{p,0}^{MM} = 3000$ , $V_{min} = 390\text{V}$ $V_{com,max} = 750\text{V}$ , $V_{com,min} = 650\text{V}$
Load Change	$k_{ac} = 2 (0.446)$ , $k_{dc} = 0.012 (0.008)$ , $r = \beta = 2000$ $d = 0.02$ , $m = 1$ , $\eta = 30$ , $\alpha = 1500$ , $l = q = 0.1$ ,
Switch	$k_{ac} = 0.039$ , $k_{dc} = 0.015 (0.005)$ , $r = \beta = 2000$ $d = 0.02$ , $m = 1$ , $\eta = 60$ , $\alpha = 1500$ , $l = q = 0.1$
Line	$R_{line}^{MTDC} = 0.5\Omega$ , $L_{line}^{MTDC} = 1.5\text{mH}$

TABLE II  
EXPERIMENTAL SYSTEM PARAMETERS

Items	Parameters & Values
AC MG	$P_{ac,max} = 10\text{kW(PV - arrays)}$ $P_{ac,load} = 6\text{kW(Light)}$ , $P_{ac,load} = 12\text{kW(Heavy)}$
DC MG	$P_{dc,max} = 10\text{kW(PV : } 5\text{kW, WT : } 5\text{kW)}$ $P_{dc,load} = 2\text{kW}$
DC-AC IC	$L = 4\text{mH}$ , $L_f = 1.8\text{mH}$ , $C_f = 25\mu\text{F}$ , $K = 6.5$ $C_{V1} = 2\text{mF}$ , $D^{AC} = 18$ , $F = 305$ , $k_P^{AC} = 3.5$ $k_I^{AC} = 187$
DC-AC IC	$L_{dc} = 1.8\text{mH}$ , $r_{dc} = 0.5\Omega$ , $D^{DC} = 68$ , $k_P^{db} = 5.8$ $k_I^{db} = 216$ , $C^{DC} = 3.2\text{mF}$ , $k_P^{DC} = 6.5$ $k_I^{DC} = 224.5$
$J$	$J_0 = 2$ , $J_{max} = 6$ , $J_{min} = 0.1$
$\Delta K_p$	$\Delta K_{p,0}^{GM} = 1500$ , $\Delta K_{p,0}^{MM} = 2400$
Load Change	$k_{ac} = 1.6$ , $k_{dc} = 0.009$ , $r = \beta = 1800$ , $\eta = 26$ $\alpha = 1300$ , $l = 0.086$ , $m = 0.8$ , $q = 0.088$ $d = 0.018$
Line	$R_{line}^{MTDC} = 0.8\Omega$ , $L_{line}^{MTDC} = 1.8\text{mH}$

REFERENCES

- [1] A. Gupta, S. Doolla and K. Chatterjee, "Hybrid AC-DC microgrid: systematic evaluation of control strategies," *IEEE Trans. Smart Grid*, vol. 9, no. 4, pp. 3830-3843, Jul. 2018.
- [2] J. Zhou, H. Zhang, Q. Sun, D. Ma and B. Huang, "Event-based distributed active power sharing control for interconnected AC and DC microgrids," *IEEE Trans. Smart Grid*, vol. 9, no. 6, pp. 6815-6828, Nov. 2018.
- [3] Y. Xia, W. Wei, M. Yu, X. Wang and Y. Peng, "Power management for a hybrid AC/DC microgrid with multiple subgrids," *IEEE Trans. Power Electron.*, vol. 33, no. 4, pp. 3520-3533, Apr. 2018.
- [4] J. M. Guerrero, M. Chandorkar, T. Lee and P. C. Loh, "Advanced control architectures for intelligent microgrids-part I: decentralized and hierarchical control," *IEEE Trans. Ind. Electron.*, vol. 60, no. 4, pp. 1254-1262, Apr. 2013.
- [5] S. Peyghami, H. Mokhtari and F. Blaabjerg, "Autonomous operation of a hybrid AC/DC microgrid with multiple interlinking converters," *IEEE Trans. Smart Grid*, vol. 9, no. 6, pp. 6480-6488, Nov. 2018.
- [6] J. Wang, C. Jin and P. Wang, "A uniform control strategy for the interlinking converter in hierarchical controlled hybrid AC/DC microgrids," *IEEE Trans. Ind. Electron.*, vol. 65, no. 8, pp. 6188-6197, Aug. 2018.
- [7] P. C. Loh, D. Li, Y. K. Chai, and F. Blaabjerg, "Autonomous operation of hybrid microgrid with AC and DC subgrids," *IEEE Trans. Power Electron.*, vol. 28, no. 5, pp. 2214-2223, May. 2013.
- [8] N. Eghtedarpour and E. Farjah, "Power control and management in a hybrid AC/DC microgrid," *IEEE Trans. Smart Grid*, vol. 5, no. 3, pp. 1494-1505, May. 2014.
- [9] S. Moayedi and A. Davoudi, "Distributed tertiary control of DC microgrid clusters," *IEEE Trans. Power Electron.*, vol. 31, no. 2, pp. 1717-1733, Feb. 2016.
- [10] A. A. A. Radwan and Y. A. I. Mohamed, "Networked control and power management of AC/DC hybrid microgrids," *IEEE Sys. Journal*, vol. 11, no. 3, pp. 1662-1673, Sept. 2017.
- [11] P. Wu, W. Huang, N. Tai, and S. Liang, "A novel design of architecture and control for multiple microgrids with hybrid AC/DC connection," *Applied Energy*, vol. 210, pp. 1002-1016, Jan. 2018.
- [12] J. Fang, H. Li, Y. Tang, and F. Blaabjerg, "On the inertia of future moreelectronics power systems," *IEEE J. Emerg. Sel. Topics Power Electron.*, vol. 7, no. 4, pp. 2130-2146, Dec. 2019.
- [13] J. Eto, J. Undrill, C. Roberts, P. Mackin, and J. Ellis, "Frequency control requirements for reliable interconnection frequency response," LBNL-2001103, Lawrence Berkley National Laboratory, Berkley, California, 2018.
- [14] Q.-C. Zhong and G. Weiss, "Synchronverters: inverters that mimic synchronous generators," *IEEE Trans. Ind. Electron.*, vol. 58, no. 4, pp. 1259-1267, Apr. 2011.

- [15] W. Wu et al., "A virtual inertia control strategy for DC microgrids analogized with virtual synchronous machines," *IEEE Trans. Ind. Electron.*, vol. 64, no. 7, pp. 6005-6016, Jul. 2017.
- [16] K. P. Schneider et al., "Improving primary frequency response to support networked microgrid operations," *IEEE Trans. Power Sys.*, vol. 34, no. 1, pp. 659-667, Jan. 2019.
- [17] G. Qi, A. Chen, and J. Chen, "Improved control strategy of interlinking converters with synchronous generator characteristic in islanded hybrid ac/dc microgrid," *CPSS Trans. Power Electron. Appl.*, vol. 2, no. 2, pp. 149-158, 2017.
- [18] E. Rakhshani and P. Rodriguez, "Inertia emulation in AC/DC interconnected power systems using derivative technique considering frequency measurement effects," *IEEE Trans. Power Syst.*, vol. 32, no. 5, pp. 3338-3351, Sep. 2017.
- [19] S. G. Vennelaganti and N. R. Chaudhuri, "Ratio-based selective inertial and primary frequency support through MTDC grids with offshore wind farms," *IEEE Trans. Power Sys.*, vol. 33, no. 6, pp. 7277-7287, Nov. 2018.
- [20] M. A. Torres, L. A. C. Lopes, L. A. Moran, and J. R. Espinoza, "Self-tuning virtual synchronous machine: A control strategy for energy storage systems to support dynamic frequency control," *IEEE Trans. Energy Convers.*, vol. 29, no. 4, pp. 833C840, Dec. 2014.
- [21] J. Alipoor, Y. Miura, and T. Ise, "Power system stabilization using virtual synchronous generator with alternating moment of inertia," *IEEE J. Emerg. Sel. Topics Power Electron.*, vol. 3, no. 2, pp. 451-458, Jun. 2015.
- [22] D. Li, Q. Zhu, S. Lin, and X. Y. Bian, "A self-adaptive inertia and damping combination control of VSG to support frequency stability," *IEEE Trans. Energy Convers.*, vol. 32, no. 1, pp. 397-398, Mar. 2017.
- [23] J. Li, B. Wen and H. Wang, "Adaptive virtual inertia control strategy of VSG for micro-grid based on improved bang-bang control strategy," *IEEE Access*, vol. 7, pp. 39509-39514, 2019.
- [24] M. Li, W. Huang, N. Tai, L. Yang, D. Duan and Z. Ma, "A dual-adaptivity inertia control strategy for virtual synchronous generator," *IEEE Trans. Power Syst.*, vol. 35, no. 1, pp. 594-604, Jan. 2020.
- [25] X. Hou, Y. Sun, X. Zhang, J. Lu, P. Wang and J. M. Guerrero, "Improvement of frequency regulation in VSG-based ac microgrid via adaptive virtual inertia," *IEEE Trans. Power Electron.*, vol. 35, no. 2, pp. 1589-1602, Feb. 2020.
- [26] Y. Wang, C. Wang, L. Xu, J. Meng and Y. Hei, "Adjustable inertial response from the converter with adaptive droop control in DC grids," *IEEE Trans. Smart Grid*, vol. 10, no. 3, pp. 3198-3209, May. 2019.
- [27] M. Hwang, E. Muljadi, G. Jang and Y. C. Kang, "Disturbance-adaptive short-term frequency support of a DFIG associated with the variable gain based on the ROCOF and rotor speed," *IEEE Trans. Power Sys.*, vol. 32, no. 3, pp. 1873-1881, May. 2017.
- [28] Y. Li et al., "A dynamic coordinated control strategy of WTG-ES combined system for short-term frequency support," *Renew. Energy*, vol. 119, pp. 1-11, Apr. 2018.
- [29] U. Markovic, Z. Chu, P. Aristidou and G. Hug, "LQR-based adaptive virtual synchronous machine for power systems with high inverter penetration," *IEEE Trans. Sustain. Energy*, vol. 10, no. 3, pp. 1501-1512, Jul. 2019.
- [30] A. S. Mir and N. Senroy, "Self-tuning neural predictive control scheme for ultrabattery to emulate a virtual synchronous machine in autonomous power systems," *IEEE Trans. Neu. Net. Lea. Sys.*, vol. 31, no. 1, pp. 136-147, Jan. 2020.
- [31] S. Samanta, J. P. Mishra and B. K. Roy, "Virtual DC machine: an inertia emulation and control technique for a bidirectional DC-DC converter in a DC microgrid," *IET Electr. Power Appl.*, vol. 12, no. 6, pp. 874-884, Jul. 2018.
- [32] Z. Li and M. Shahidehpour, "Small-Signal Modeling and Stability Analysis of Hybrid AC/DC Microgrids," *IEEE Trans. Smart Grid*, vol. 10, no. 2, pp. 2080-2095, Mar. 2019.
- [33] D. Xue and Y. Chen, "Advanced applied mathematical problem solutions with MATLAB," Tsinghua University Press, Beijing, China, 2018.



**Yi Zhang** received the B.S. degree in electrical engineering and automation from the Henan Normal University, China, in 2016 and the M.S. degree in electrical engineering from the Northeastern University, Shenyang, in 2018. She is currently pursuing his Ph.D. degree in the School of Information Science and Engineering, Northeastern University, China.

Her research interests are stability analysis of microgrid, power quality improvement of microgrids and Energy Internet.



**Qiuye Sun** (M'11-SM'19) received the Ph.D. degree in 2007. He is currently a full Professor with Northeastern University and obtained Special Government Allowances from the State Council in China. He has authored or coauthored over 200 papers, authorized over 100 invention patents, and published over 10 books or textbooks.

He is an Associate Editor of IEEE Transactions on Neural Networks and Learning Systems, IET Cyber-Physical Systems, CSEE Journal of Power and Energy Systems, IEEE/CAA Journal of Automatica Sinica, Journal of Control and Decision and so on. His current research interests include optimization analysis technology of power distribution network, network control of Energy Internet, Integrated Energy Systems and Microgrids.



**Jianguo Zhou** (M'19) received the B.S. degree in automation and the M.S. and Ph.D. degrees in control theory and control engineering from Northeastern University, Shenyang, China, in 2011, 2013 and 2018, respectively.

Since 2018, he has been a postdoctoral researcher with the Tsinghua-Berkeley Shenzhen Institute (TBSI), Tsinghua Shenzhen International Graduate School (TsinghuaSIGS), Tsinghua University, Shenzhen, China. His current research interests include distributed control and optimization with applications in microgrids, Energy Internet and integrated energy systems.



**Linjuan Li** received the B.S. degree in electrical engineering and automation from the Shenyang Agricultural University, China, in 2017 and the M.S. degree in electric power system and automation from the Northeastern University, Shenyang, China, in 2020.

Her research interests are control of power converters, distributed microgrid and power electronic enabled power network.



**Panfeng Wang** received the B.S. degree in electrical engineering and automation from Northeastern University, Shenyang, China, in 2017. He is currently pursuing his M.S. degree in the School of Information Science and Engineering, Northeastern University, China.

His research interests are power converters for renewable energy source, distributed cooperative control and their applications in microgrids.



**Josep M. Guerrero** ((S'01-M'04-SM'08-FM'15) received the B.S. degree in telecommunications engineering, the M.S. degree in electronics engineering, and the Ph.D. degree in power electronics from the Technical University of Catalonia, Barcelona, in 1997, 2000 and 2003, respectively. Since 2011, he has been a Full Professor with the Department of Energy Technology, Aalborg University, Denmark, where he is responsible for the Microgrid Research Program. From 2014 he is chair Professor in Shandong University; from 2015 he is a distinguished

guest Professor in Hunan University; and from 2016 he is a visiting professor fellow at Aston University, UK, and a guest Professor at the Nanjing University of Posts and Telecommunications. From 2019, he became a Villum Investigator by The Villum Fonden, which supports the Center for Research on Microgrids (CROM) at Aalborg University, being Prof. Guerrero the founder and Director of the same centre ([www.crom.et.aau.dk](http://www.crom.et.aau.dk)).

His research interests is oriented to different microgrid aspects, including power electronics, distributed energy-storage systems, hierarchical and cooperative control, energy management systems, smart metering and the internet of things for AC/DC microgrid clusters and islanded minigrids. Specially focused on microgrid technologies applied to offshore wind, maritime microgrids for electrical ships, vessels, ferries and seaports, and space microgrids applied to nanosatellites and spacecrafts. Prof. Guerrero is an Associate Editor for a number of IEEE TRANSACTIONS. He has published more than 600 journal papers in the fields of microgrids and renewable energy systems, which are cited more than 50,000 times. He received the best paper award of the IEEE Transactions on Energy Conversion for the period 2014-2015, and the best paper prize of IEEE-PES in 2015. As well, he received the best paper award of the Journal of Power Electronics in 2016. During six consecutive years, from 2014 to 2019, he was awarded by Clarivate Analytics (former Thomson Reuters) as Highly Cited Researcher with 50 highly cited papers. In 2015 he was elevated as IEEE Fellow for his contributions on “distributed power systems and microgrids.”